AGU PUBLICATIONS

Paleoceanography

RESEARCH ARTICLE
10.1002/2015PA002833

Key Points:
- Foraminifer O. umbonatus Mg/Ca has low sensitivity to changing seawater Mg/Ca
- Greater than modern ice volume followed Middle Miocene Climate Transition
- Plio-Pleistocene glaciation preceded by a change in Pacific Ocean overturning

Supporting Information:
- Text S1, Figures S1–S6, and Tables S1–S5

Correspondence to:
C. H. Lear,
learc@cardiff.ac.uk

Citation:
Lear, C. H., H. K. Coxall, G. L. Foster, D. J. Lunt, E. M. Mawbey, Y. Rosenthal, S. M. Sosdian, E. Thomas, and P. A. Wilson (2015), Neogene ice volume and ocean temperatures: Insights from infaunal foraminiferal Mg/Ca paleothermometry, *Paleoceanography*, *30*, doi:10.1002/2015PA002833.

Received 12 MAY 2015
Accepted 5 OCT 2015
Accepted article online 14 OCT 2015

Neogene ice volume and ocean temperatures: Insights from infaunal foraminiferal Mg/Ca paleothermometry

Caroline H. Lear[1], Helen K. Coxall[2], Gavin L. Foster[3], Daniel J. Lunt[4], Elaine M. Mawbey[1], Yair Rosenthal[5], Sindia M. Sosdian[1], Ellen Thomas[6], and Paul A. Wilson[3]

[1]School of Earth and Ocean Sciences, Cardiff University, Cardiff, UK, [2]Department of Geological Sciences, Stockholm University, Stockholm, Sweden, [3]National Oceanography Centre Southampton, University of Southampton, Southampton, UK, [4]School of Geographical Sciences, Bristol University, Bristol, UK, [5]Institute of Marine and Coastal Sciences and Department of Geological Sciences, Rutgers, State University of New Jersey, New Brunswick, New Jersey, USA, [6]Department of Geology and Geophysics, Yale University, New Haven, Connecticut, USA

Abstract Antarctic continental-scale glaciation is generally assumed to have initiated at the Eocene-Oligocene Transition, yet its subsequent evolution is poorly constrained. We reconstruct changes in bottom water temperature and global ice volume from 0 to 17 Ma using $\delta^{18}O$ in conjunction with Mg/Ca records of the infaunal benthic foraminifer, *O. umbonatus* from Ocean Drilling Program (ODP) Site 806 (equatorial Pacific; ~2500 m). Considering uncertainties in core top calibrations and sensitivity to seawater Mg/Ca $(Mg/Ca)_{sw}$, we produce a range of Mg/Ca-temperature-Mg/Ca_{sw} calibrations. Our favored exponential temperature calibration is $Mg/Ca = 0.66 \pm 0.08 \times Mg/Ca_{sw}^{0.27\pm0.06} \times e^{(0.114\pm0.02 \times BWT)}$ and our favored linear temperature calibration is $Mg/Ca = (1.21 \pm 0.04 + 0.12 \pm 0.004 \times BWT$ (bottom water temperature)) $\times (Mg/Ca_{sw}^{-0.003\pm0.02})$ (stated errors are 2 s.e.). The equations are obtained by comparing *O. umbonatus* Mg/Ca for a Paleocene-Eocene section from Ocean Drilling Program (ODP) Site 690 (Weddell Sea) to $\delta^{18}O$ temperatures, calculated assuming ice-free conditions during this peak warmth period of the Cenozoic. This procedure suggests negligible effect of Mg/Ca_{sw} on the Mg distribution coefficient (D_{Mg}). Application of the new equations to the Site 806 record leads to the suggestion that global ice volume was greater than today after the Middle Miocene Climate Transition (~14 Ma). ODP Site 806 bottom waters cooled and freshened as the Pacific zonal sea surface temperature gradient increased, and climate cooled through the Pliocene, prior to the Plio-Pleistocene glaciation of the Northern Hemisphere. The records indicate a decoupling of deep water temperatures and global ice volume, demonstrating the importance of thresholds in the evolution of the Antarctic ice sheet.

1. Introduction

The cryosphere affects climate through changing ocean/atmosphere heat transport and biogeochemical carbon cycling. Accurate records of the cryosphere and corresponding paleoceanographic conditions are required to understand how these processes contributed to the evolution of Earth's climate through the Cenozoic. Records of ice-rafted debris and continental weathering suggest that semipermanent Antarctic continental-scale glaciation initiated at the Eocene-Oligocene climate transition (EOT), ~34 Ma [*Zachos et al.*, 1992; *Scher et al.*, 2011]. The history of the development of continental-scale ice sheets in the Northern Hemisphere is more controversial, but Northern Hemisphere glaciation probably occurred later [*Edgar et al.*, 2007; *DeConto et al.*, 2008]. Iceberg-derived dropstones have been documented in the Norwegian Greenland Sea from EOT time but are likely sourced from isolated coastal mountain outlet glaciers on Greenland [*Eldrett et al.*, 2007], whereas major Pleistocene Northern Hemisphere glaciation apparently began around 2.6 Ma [*Raymo et al.*, 1989; *Bailey et al.*, 2013]. The Cenozoic benthic foraminiferal oxygen isotope compilation delineates the nonlinear transition from the greenhouse world of the early Cenozoic to today's icehouse world [*Shackleton and Kennett*, 1975; *Miller et al.*, 1987; *Zachos et al.*, 2001, 2008; *Cramer et al.*, 2009; *Mudelsee et al.*, 2014]. This record reflects deep-sea temperatures in addition to global ice volume. Three $\delta^{18}O$ "steps" have been interpreted as significant ice sheet growth events, as the climate system crossed key thresholds [*Zachos et al.*, 1996, 2001, 2008; *DeConto et al.*, 2008]. The earliest "step" at the EOT is recognized as reflecting the continent-wide glaciation on Antarctica [*Zachos et al.*, 1992; *Lear et al.*, 2000; *Coxall et al.*, 2005; *Scher et al.*, 2011]. The second step is the Middle Miocene Climate Transition

(MMCT), around 14 Ma [*Holbourn et al*., 2005]. Backstripping estimates suggest that sea level fell between 53 and 69 m between 16.5 and 13.9 Ma [*John et al*., 2011]. Glacial landforms provide evidence of larger-than-modern ice sheets overriding the Transantarctic Mountains during the middle Miocene [*Denton and Sugden*, 2005]. The MMCT has been linked to ice sheet advance and a transition from a polythermal to a dry-based Antarctic ice sheet [*Lewis et al*., 2007], as levels of CO_2 decreased and orbital configurations favored low seasonality at high latitudes [*Holbourn et al*., 2005, 2007; *Foster et al*., 2012]. Following the MMCT, the Antarctic ice sheet may have been less sensitive to changes in high-latitude radiative forcing, with ice volume controlled more by variations in moisture transport [*Holbourn et al*., 2013a]. The most recent step in the $\delta^{18}O$ record largely reflects the Plio-Pleistocene intensification of glaciation in the Northern Hemisphere. However, the dual control of temperature and ice volume on foraminiferal $\delta^{18}O$ means that significant questions regarding the extent of continental glaciation and the relationship between the crysophere and ocean overturning circulation through the Neogene remain.

Benthic foraminiferal Mg/Ca paleothermometry has shown great promise in deconvolving the temperature and $\delta^{18}O_{sw}$ signal from foraminiferal $\delta^{18}O$ records, although it is not without its complications [*Lear et al*., 2000, 2010; *Billups and Schrag*, 2002, 2003; *Martin et al*., 2002; *Shevenell et al*., 2008; *Cramer et al*., 2011; *Bohaty et al*., 2012]. Chiefly, these are as follows: (1) variations in Mg/Ca temperature sensitivity between foraminiferal genera necessitating genus- or species-specific temperature calibrations [*Lear et al*., 2002], (2) the influence of carbonate saturation state at low saturation [*Elderfield et al*., 2006], (3) uncertainties in seawater Mg/Ca reconstructions [*Coggon et al*., 2010], and (4) the relationship between seawater Mg/Ca and foraminiferal calcite Mg/Ca [*Hasiuk and Lohmann*, 2010; *Ries*, 2004; *Cramer et al*., 2011; *Evans and Müller*, 2012]. The last two complications do not compromise the use of Mg/Ca paleothermometry on short ($<$1 Myr) timescales, making the proxy ideally suited to examining relative temperature changes over geologically short time intervals [*Lear et al*., 2008; *Elderfield et al*., 2012; *Mawbey and Lear*, 2013]. However, over longer timescales they limit the reconstruction of absolute temperatures, which are required to estimate absolute ice volume from $\delta^{18}O$. Previous efforts to address these issues have been informative, but progress has been limited by a paucity of available Mg/Ca records [*Cramer et al*., 2011; *Evans and Müller*, 2012]. The saturation state influence is of particular importance for epifaunal foraminifera, which more directly experience changing bottom water mass chemistry.

Here we present a record of benthic foraminiferal Mg/Ca for the past 17 Ma and attempt to minimize or address these factors in order to calculate absolute bottom water temperature (BWT) and $\delta^{18}O_{sw}$ for the late Neogene. All records are from one species, the shallow infaunal dwelling *Oridorsalis umbonatus*, for which core top calibrations exist [*Lear et al*., 2002; *Rathmann et al*., 2004; *Healey et al*., 2008; *Brown et al*., 2011; *Tisserand et al*., 2013]. We minimize the influence of the bottom water carbonate saturation state [*Elderfield et al*., 2010] by using an infaunal species living within the upper few centimeters of the seafloor sediment, and by careful site selection, avoiding sites below the lysocline where foraminifera may experience postmortem dissolution. We also present a new Mg/Ca record from the ice-free early Paleogene, for which bottom water temperatures can be independently calculated from $\delta^{18}O$, representing a time of far lower seawater Mg/Ca than today. We combine this record with published core top Mg/Ca data to better constrain the relationship between seawater Mg/Ca and foraminiferal Mg/Ca for this species. We find that *Oridorsalis umbonatus* has a low sensitivity to changes in seawater Mg/Ca, implying a strong biological control on its calcification process. We then interpret our Neogene Mg/Ca and $\delta^{18}O$ records in terms of absolute BWT and $\delta^{18}O_{sw}$ and find strong support for greater than modern ice volume immediately following the Middle Miocene Climate Transition and a change in ocean overturning circulation associated with late Neogene global cooling.

2. Materials and Methods

2.1. Advantages of Infaunal Foraminifera in Mg/Ca Paleothermometry

Benthic foraminiferal Mg/Ca is primarily controlled by changes in bottom water temperature [*Rosenthal et al*., 1997; *Lear et al*., 2002; *Marchitto et al*., 2007]. However, the degree of carbonate saturation (ΔCO_3^{2-}) impacts benthic foraminiferal Mg/Ca at low saturation [*Elderfield et al*., 2006; *Rosenthal et al*., 2006]. Initial work focused on the epifaunal taxon *Cibicidoides*, which lives above, at, or very close to the seafloor in direct contact with bottom water [*Jorissen et al*., 2007]. Mg/Ca in infaunal benthic foraminifera might be a more reliable paleotemperature proxy, because pore waters are buffered to some extent against changes in carbonate

saturation [*Elderfield et al*., 2010]. Oxidation of sedimentary organic matter tends to decrease the pore water carbonate saturation state. Once pore waters become undersaturated, dissolution of carbonate grains buffers against further decreases in saturation state [*Zeebe*, 2007].

To address the saturation state problem in the Pleistocene, a Mg/Ca temperature record based on the infaunal genus *Uvigerina* from Ocean Drilling Program (ODP) Site 1123 (3.3 km water depth on Chatham Rise, east of New Zealand) has been used to calculate Pleistocene changes in $\delta^{18}O_{sw}$. Remarkable agreement with independent sea level proxies provides strong support for the validity of this approach [*Elderfield et al*., 2012; *Rohling et al*., 2014]. We take the same approach using *Oridorsalis umbonatus*, an extant shallow infaunal species, found globally through the Late Cretaceous-Cenozoic, for which core top calibrations exist [*Lear et al*., 2002; *Rathmann et al*., 2004; *Healey et al*., 2008; *Brown et al*., 2011; *Tisserand et al*., 2013]. Core top and down core records suggest that this species, like *Uvigerina* species, is less sensitive to changes in bottom water saturation state than epifaunal species [*Brown et al*., 2011; *Mawbey and Lear*, 2013; *Foster et al*., 2013]. However, the trace metal composition of *O. umbonatus* appears sensitive to changes in carbonate saturation state in some instances, so we cannot assume that *O. umbonatus* is consistently and fully buffered from changes in bottom water saturation state in its microhabitat. For example, Mg/Ca in *O. umbonatus* increases by 0.28 mmol/mol across the EOT at ODP Site 1218 [*Lear et al*., 2004], which is surprising given the widespread cooling associated with the major Antarctic glaciation [*Liu et al*., 2009]. However, at ODP Site 1218 the EOT is also associated with extensive (~1.2 km) deepening of the calcite compensation depth, a lithologic change from radiolarite to nannofossil oozes and chalks, and thus an increase in pore water buffering capacity of this deep ocean site (paleowater depth ~3800 m) [*Coxall et al*., 2005; *Lyle et al*., 2002]. Possibly, the very low carbonate saturation state at this site influenced the benthic foraminiferal Mg/Ca through a combination of effects during test precipitation and postmortem dissolution (many tests, especially from samples taken from the upper Eocene radiolarites contain dissolution pits).

2.2. Site Selection

We cannot assume that all infaunal foraminifera, living at various depths within the sediment from close to the surface to >10 cm deep [*Jorissen et al*., 2007] inhabit pore waters that are fully buffered with respect to carbonate saturation state, so sites for infaunal Mg/Ca paleothermometry should be selected carefully. The presence of abundant, well-preserved planktonic foraminifera is one indication that sediment can buffer pore waters against significant decreases in carbonate saturation state. Sediment pore water chemistry under regions of vigorous upwelling may be complicated by temporal variations in organic matter degradation, and pore waters thus may not be fully buffered [*Rathmann and Kuhnert*, 2008]. In addition, hiatuses in sedimentation or transient dissolution events may disrupt the buffering capacity of the pore waters [*Mawbey and Lear*, 2013]. Therefore, we selected carbonate-rich samples with abundant planktonic foraminifera. In order to maximize the potential dissolution capacity of the sediments, we have selected samples from paleowater depths of less than 3 km.

Our new benthic foraminiferal Mg/Ca and $\delta^{18}O$ data between ~17 and 12 Ma span the MMCT at Ocean Drilling Program (ODP) Site 806, presently at 2521 m water depth on the Ontong Java Plateau in the Pacific Ocean (0°19.1′N 159°21.7′E) (Figure 1). Carbonate contents for these sediments are typically between 90 and 95% [*Kroenke et al*., 1991]. Detailed stable isotope records from ~13.3 to 14.1 Ma on an orbitally tuned age model are presented in *Holbourn et al*. [2013b]. We combine our Site 806 record with previously published *O. umbonatus* data from upper Miocene to Pleistocene strata from the same site [*Lear et al*., 2003]. We also present new benthic foraminiferal Mg/Ca data from the upper Paleocene to lower Eocene from ODP Site 690, present water depth 2914 m, on Maud Rise in the Southern Ocean (65°9.629′S, 1°12.30′E) (Figure 1). The sediments typically contain between 75 and 95% carbonate and have abundant planktonic foraminifera [*Barker et al*., 1988]. These strata show sedimentation rates of ~1–2 cm/kyr and are estimated to have been deposited at a paleowater depth of 1900 m [*Barker et al*., 1988; *Thomas and Shackleton*, 1996]. Therefore, we assume that the pore waters were buffered with respect to carbonate saturation state. Our age model for Site 806 uses nannofossil biostratigraphic events [*Nathan and Leckie*, 2009] and planktonic foraminiferal events [*Kroenke et al*., 1991] assigned to ages provided in *Wade et al*. [2011] (Figure S1 in the supporting information). For ODP Site 690 we correlated carbon isotope events to the record from ODP Site 1262 on Walvis Ridge, so our ages are consistent with those of *Littler et al*. [2014] (depths and ages are provided in the supporting information).

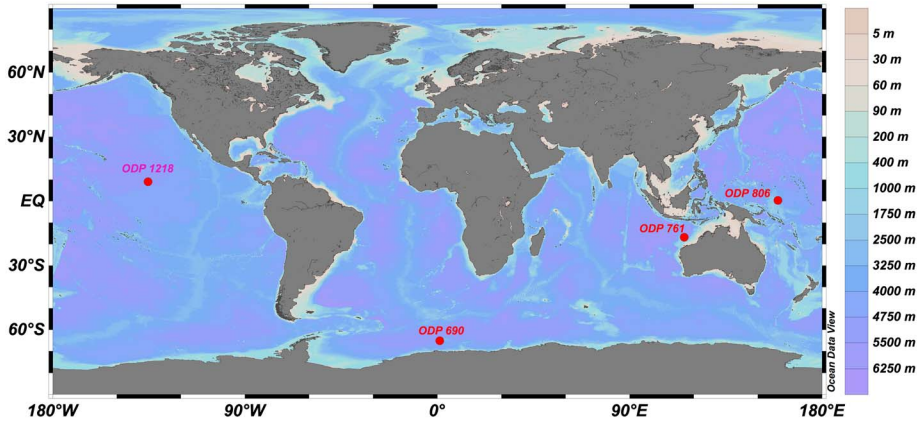

Figure 1. Locations of sites studied.

2.3. Stable Isotopes

For the ODP Site 806 MMCT samples, approximately six individuals of *Cibicidoides* spp (250–355 μm) were crushed, ultrasonicated in methanol to remove clays and oxidized with 3% H_2O_2 to remove organic matter. Samples were analyzed on a ThermoFinnigan MAT252 with online sample preparation using an automated Kiel III carbonate device at Cardiff University. Results are reported relative to Pee Dee Belemnite, and long-term uncertainty based on repeat analysis of NBS-19 is ±0.08‰ (2σ). Data are provided in Table S1 in the supporting information.

2.4. Trace Element Analysis

The Site 806 MMCT samples were cleaned using the same protocol as that used for the upper Miocene to Pleistocene record of *Lear et al.* [2003]. Between three and ten individuals of the benthic foraminifer *O. umbonatus* were picked from the 250–355 μm size fraction and crushed between glass plates to open all chambers. Test fragments were cleaned using a protocol to remove clays, metal oxides, and organic matter [*Boyle and Keigwin*, 1985]. Between the clay removal and reductive steps the samples were examined under a binocular microscope, and noncarbonate particles were removed using a fine paintbrush. Samples were dissolved in trace metal pure 0.065 M HNO_3 and diluted with trace metal pure 0.5 M HNO_3 to a final volume of 350 μL. Samples were analyzed at Cardiff University on a Thermo Element XR ICP-MS against standards with matched calcium concentration to reduce matrix effects [*Lear et al.*, 2002]. All data for a sample were rejected if Al/Ca exceeded 50 μmol/mol, Mn/Ca exceeded 100 μmol/mol or Fe/Ca exceeded 200 μmol/mol. B/Ca data were rejected if the sample boron intensity signal was less than 10 times that of the blank. Long-term precision as determined by analyzing an independent consistency standard during each run is ~1% and 5% (relative standard deviation) for Mg/Ca and B/Ca respectively. The ODP Site 690 Paleocene-Eocene samples were cleaned without the reductive step and analyzed using a Varian Vista ICP-OES at Cambridge University, with a precision of <1% for Mg/Ca. To achieve consistency between data sets, 9.1% was subtracted from the Mg/Ca data from ODP Site 690 [*Yu et al.*, 2007]. Trace metal data are available in Tables S1 and S2 of the supporting information.

3. Results

3.1. ODP Site 806 Middle Miocene Record

Our oxygen isotope stratigraphy displays the global ~1‰ shift to heavier values across the Middle Miocene Climate Transition and is consistent with the shorter duration, high-resolution record of *Holbourn et al.* [2013b]. The 12–17 Ma Miocene Mg/Ca record presented here appears consistent with the previously published record for 0–11 Ma from the same site (Figure 2) [*Lear et al.*, 2003]. Mg/Ca is variable and high within the Miocene Climatic Optimum (~15–17 Ma). Following the MMCT, Mg/Ca was lower and more stable at around 2 mmol/mol until ~5 Ma (Figure 2). After ~5 Ma Mg/Ca decreased by ~0.6 mmol/mol (Figure 2). Middle Miocene *O. umbonatus* Mg/Ca values at ODP Site 806 are on average 0.4 mmol/mol lower than those at ODP Site 761 (Wombat Plateau; 2179 m) (Figure 3) [*Lear et al.*, 2010].

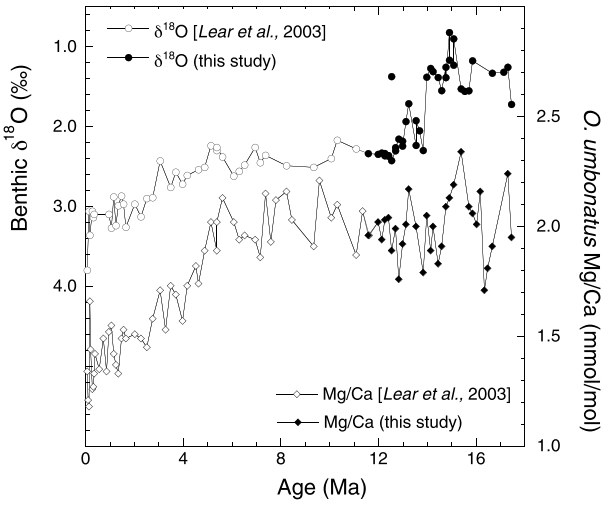

Figure 2. Benthic foraminiferal oxygen isotope ($\delta^{18}O$, circles) and Mg/Ca (diamonds) records from ODP Site 806. Open symbols are previously published [*Lear et al*., 2003], closed symbols are from this study.

3.2. ODP Site 690 Paleocene-Eocene Record

Our *O. umbonatus* Mg/Ca record from ODP Site 690 increases as benthic foraminiferal $\delta^{18}O$ decreases (Figure 4a). Maximum Mg/Ca values occurred around 52.8 Ma, close to Eocene Thermal Maximum 2, since no data were included from the Paleocene-Eocene Thermal Maximum (Figure 4b) [*Zachos et al*., 2008]. We compile the *Cibicidoides* and *Nuttallides* $\delta^{18}O$ data from *Kennett and Stott* [1990] and *Thomas and Shackleton* [1996], using the species offsets in *Katz et al*. [2003], correlated to the record in *Littler et al*. [2014] to create an isotope stratigraphy for ODP Site 690 (Figure 4a). We then use linear interpolation to estimate an equivalent equilibrium $\delta^{18}O$ value for each of our Mg/Ca samples (Figure 4b). Assuming an ice-free value for $\delta^{18}O_{sw}$ of −0.89‰ [*Cramer et al*., 2011], we calculated bottom water temperatures (BWTs) for the interpolated $\delta^{18}O$ values, using the quadratic oxygen isotope paleotemperature equation of *Marchitto et al*. [2014]. The Mg/Ca data display a positive trend with these $\delta^{18}O$ paleotemperatures, with a slope of 0.09 ± 0.04 mmol/mol/°C (2 s.e., $r^2 = 0.6$) (Figure 4c), within the error of the 0.12 ± 0.01 mmol/mol/°C (2 s.e., $r^2 = 0.9$) sensitivity of a previous calibration based on a core top *O. umbonatus* and *C. pachyderma* data set [*Marchitto et al*., 2007; *Lear et al*., 2010]. The value for the oldest sample at 57.1 Ma is perhaps slightly higher than expected from temperature alone (Figure 4b). This is likely caused, at least in part, by natural variability in the Mg/Ca record, and the interspecies interpolation process (compare Figures 4a and 4b), although we cannot rule out the possibility of higher seawater Mg/Ca in this part of the record. However, the slope in Figure 4c is unchanged if this sample is omitted.

4. Discussion

4.1. Constraining the Sensitivity of Mg/Ca in *O. umbonatus* to Changes in Seawater Mg/Ca

Seawater Mg/Ca (Mg/Ca_{sw}) values have increased from around 1.5 mol/mol in the early Cenozoic to today's value of 5.2 mol/mol [*Coggon et al*., 2010; *Dickson*, 2002; *Horita et al*., 2002]. The residence times of Ca and Mg in seawater (~1 Myr and ~10 Myr, respectively) [*Broecker and Peng*, 1982] means that potential changes in Mg/Ca_{sw} need to be taken into account when calculating absolute BWT through the Cenozoic. Earlier studies assumed that benthic foraminiferal Mg/Ca was linearly related to seawater Mg/Ca [*Lear et al*., 2000; *Billups and Schrag*, 2003], but more recent culture studies on a range of calcifying organisms suggest that the relationship is better described by a power law dependency (equation (1)) [*Ries*, 2004],

$$Mg/Ca_{cc} = F \times Mg/Ca_{sw}{}^{H} \quad (1)$$

where Mg/Ca_{cc} is the Mg/Ca of the calcite, Mg/Ca_{sw} is the Mg/Ca of seawater, and F is a factor that could include a linear or exponential temperature dependency. A culture study of the planktonic foraminifer *Globigerinoides sacculifer* did not produce a clear relationship between Mg/Ca_{cc} and Mg/Ca_{sw} [*Delaney et al*., 1985]. Culture studies of the larger, high-Mg calcite, symbiont-bearing benthic foraminiferal species *Amphistegina lobifera*, *Amphistegina lessonii*, and *Heterostegina depressa* found values for *H* of 0.8, 0.7–0.8, and 0.44, respectively [*Segev and Erez*, 2006; *Raitzsch et al*., 2010; *Mewes et al*., 2014]. The shallow water, low-Mg calcite foraminifer *Ammonia aomoriensis* has an *H* value of 0.7 [*Mewes et al*., 2014]. While it is clear that there are species differences, it is not known whether these values for H would be similar for other benthic foraminiferal species such as *O. umbonatus*, which calcifies in deep ocean waters at lower saturation states.

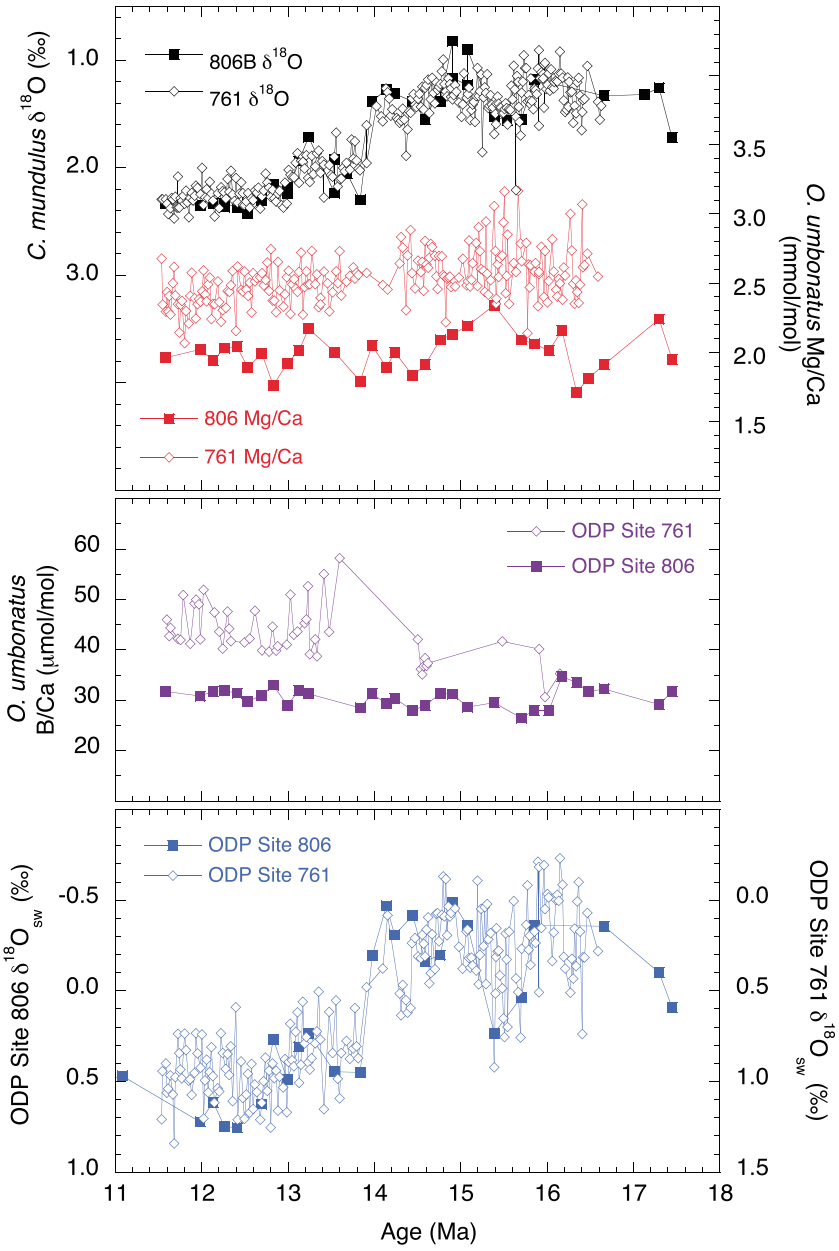

Figure 3. Benthic foraminiferal $\delta^{18}O$ (black), Mg/Ca (red), B/Ca (purple), and $\delta^{18}O_{sw}$ (blue) records from ODP Site 761 (open diamonds) and ODP Site 806 (closed squares). ODP Site 761 $\delta^{18}O$ and Mg/Ca data from *Lear et al.* [2010] and ODP Site 806 data from *Lear et al.* [2003] and this study. $\delta^{18}O_{sw}$ calculated using the *Lear et al.* [2002] Mg/Ca temperature sensitivity assuming early Eocene $Mg/Ca_{sw} = 1.3$ (Table 1) and the oxygen isotope paleotemperature equation of *Marchitto et al.* [2014]. The $\delta^{18}O_{sw}$ values from ODP Site 761 are biased toward heavy values as a result of the elevated Mg/Ca (see text for details).

An alternative approach to constraining the relationship between foraminiferal Mg/Ca and seawater Mg/Ca is to use fossil foraminifera that precipitated their tests in seawater with different Mg/Ca values than modern. This approach assumes that the Mg/Ca of the fossil foraminifera has not been diagenetically altered. Benthic foraminifera are less porous and thus less susceptible to postdepositional alteration than planktonic foraminifera [*Edgar et al.*, 2013]. The species *Oridorsalis umbonatus* has minute pores (e.g., much smaller than *Nuttallides truempyi*) and thus is among the least susceptible benthic species [*Foster et al.*, 2013], but we acknowledge this potential uncertainty. This approach also requires knowledge of the ancient seawater Mg/Ca, BWT, and the species-specific Mg/Ca temperature sensitivity. BWT can be estimated using

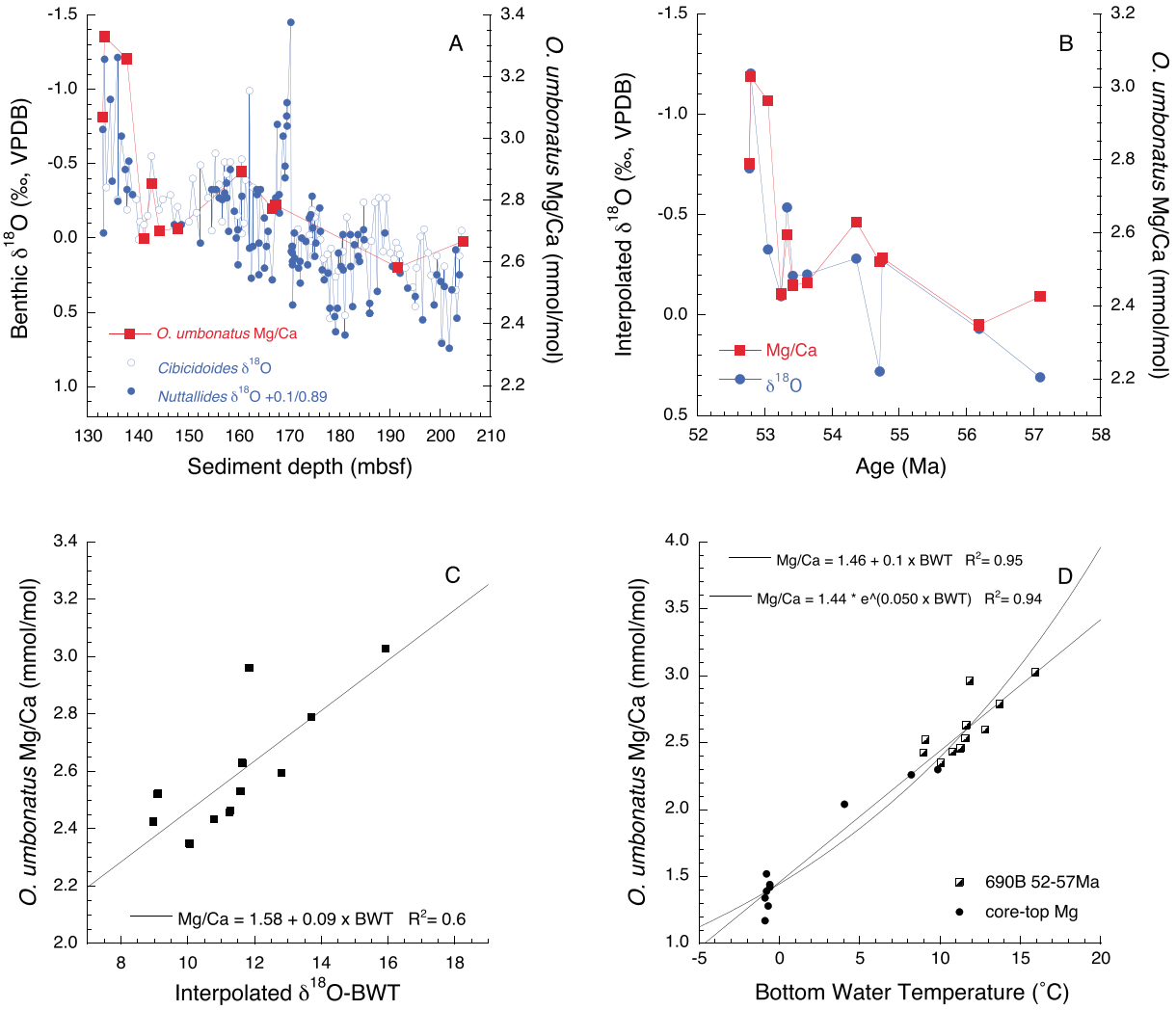

Figure 4. (a) Benthic foraminiferal oxygen isotope (blue) and unadjusted Mg/Ca (red) versus sediment burial depth (meters below seafloor) at ODP Site 690. Oxygen isotope data are from *Kennett and Stott* [1990] and *Thomas and Shackleton* [1996], Mg/Ca data are from this study. (b) Benthic foraminiferal Mg/Ca and linearly interpolated oxygen isotope data from Figure 4a versus age. Mg/Ca data have been adjusted by −9.1% to correct for the short cleaning procedure. (c) Adjusted benthic foraminiferal Mg/Ca versus interpolated $\delta^{18}O$−temperature, calculated assuming $\delta^{18}O_{sw}$ =−0.89 (SMOW). (d) Benthic foraminiferal Mg/Ca versus temperature, data combined from Figure 4c (squares) and core top data used in the NS-LBB calibrations (circles) (see text for details). Mg/Ca data from Site 690 have been adjusted by −9.1% to correct for the short cleaning procedure (see text for details).

benthic foraminiferal $\delta^{18}O$ if $\delta^{18}O_{sw}$ is independently known. The greenhouse world of the early Eocene is generally thought to have been ice-free, with $\delta^{18}O_{sw}$ of -0.89 ± 0.02‰ (SMOW) [*Cramer et al*., 2011]. With Mg/Ca_{sw} very different from modern (<2 versus 5.2, [*Dickson*, 2002]), this provides an ideal interval to assess the relationship between foraminiferal Mg/Ca and seawater chemistry [*Lear et al*., 2002; *Billups and Schrag*, 2003; *Cramer et al*., 2011; *Evans and Müller*, 2012]. *Cramer et al*. [2011] normalized published multispecies benthic foraminiferal Mg/Ca records to a single species, then applied both a "water depth correction" and a "calcite compensation depth" correction for the potential influence of the carbonate saturation state. This approach assumes a linear relationship between benthic foraminiferal Mg/Ca and carbonate saturation state without a threshold, which is unlikely [*Yu and Elderfield*, 2008]. For *O. umbonatus*, *Cramer et al*. [2011] estimated $H = 0.03$ using the Mg/Ca temperature sensitivity of *Lear et al*. [2010] and $H = 0.7$ using the Mg/Ca temperature sensitivity of *Rathmann et al*. [2004]. The Mg/Ca temperature sensitivity of *Lear et al*. [2002] produced a value of 0.4–0.6 for *O. umbonatus*, [*Evans and Müller*, 2012; D. Evans, personal communication, 2014].

Here we attempt to improve upon these estimates. First, for our Paleogene samples, we use Mg/Ca and $\delta^{18}O$ data from the same site to reduce the uncertainty associated with BWT estimates. Second, we use a range of samples from peak greenhouse conditions (52–57 Ma) rather than sparse data from ~48 Ma [*Lear et al*., 2000; *Evans and Müller*, 2012]. This improves our confidence in the assumption of an ice-free world. Third, rather than combining epifaunal and infaunal Mg/Ca records, we use only the infaunal species *O. umbonatus*. Finally, we do not introduce an ad hoc correction for carbonate saturation state [*Cramer et al*., 2011] but focus on ODP Site 690, a carbonate-rich site at an intermediate paleowater depth, which shows relatively minor dissolution even during the extreme dissolution of the Paleocene-Eocene Thermal Maximum [*Thomas*, 1998; *Zeebe and Zachos*, 2007; *Kelly et al*., 2012]. We therefore assume that *O. umbonatus* precipitated its calcite test in pore waters buffered against changes in carbonate saturation state at ODP Site 690 in the Paleogene.

We assume that the *O. umbonatus* Mg/Ca temperature Mg/Ca_{sw} relationship has one of two forms, depending on whether the Mg/Ca temperature relationship is best described as an exponential or linear relationship [*Ries*, 2004]:

$$Mg/Ca = A \cdot Mg/Ca_{sw}{}^{H} \cdot \exp^{(B \times BWT)} \quad (2)$$

or

$$Mg/Ca = (c + m \cdot BWT) \cdot Mg/Ca_{sw}{}^{H} \quad (3)$$

Values for *A*, *B*, *C*, *m*, and *H* can be calculated by solving each equation simultaneously to satisfy both the Paleocene-Eocene data set (Figure 4) and the Mg/Ca temperature relationship in core top samples, for which $Mg/Ca_{sw} = 5.2$. This approach is sensitive to the choice of Mg/Ca temperature calibration [*Cramer et al*., 2011].

The first *O. umbonatus* Mg/Ca temperature calibration is based on core top data from the North Atlantic, offshore Hawaii, Gulf of California, Sea of Okhotsk, Southern Ocean, and Little Bahama Banks [*Lear et al*., 2002]. An exponential curve fit through the data spans a temperature range of 0.8 to 9.9°C (equation (4)).

$$Mg/Ca = 1.008 \pm 0.08 \times \exp(0.114 \pm 0.02 \times BWT),\ n = 23,\ R^2 = 0.4 \quad (4)$$

A later calibration was based on core top *O. umbonatus* Mg/Ca along a depth transect off the Namibia coast spanning a temperature range of 2.9–10.4°C [*Rathmann et al*., 2004]. This study found a similar temperature sensitivity, but with Mg/Ca apparently offset by around +0.5 mmol/mol (equation (5)).

$$Mg/Ca = 1.528 \times \exp(0.09 \times BWT) \quad (5)$$

The *Lear et al*. [2002] core top data set used foraminifera that had been oxidatively and reductively cleaned, whereas the *Rathmann et al*. [2004] data set is based on laser ablation analyses of noncleaned foraminifera. Direct comparison of the absolute values is therefore not trivial, yet the similarity in temperature sensitivities is encouraging. However, a study of core top *O. umbonatus* Mg/Ca from deep ocean sites with temperatures <4°C [*Healey et al*., 2008] estimated a temperature sensitivity more than double that of *Lear et al*. [2002] (equations (6) and (7)). It seems more than likely that this sensitivity is high because of the influence of low carbonate saturation states on Mg/Ca [*Healey et al*., 2008].

$$Mg/Ca = 0.988 \pm 0.08 \times \exp(0.252 \pm 0.036 \times BWT) \quad (6)$$

$$Mg/Ca = 0.449 \pm 0.066 \times BWT + 0.773 \pm 0.151 \quad (7)$$

Lear et al. [2010] provide further *O. umbonatus* Mg/Ca core top data from the Norwegian and Timor Seas and combined core top *O. umbonatus* and *C. pachyderma* data [*Marchitto et al*., 2007] to produce a linear Mg/Ca temperature calibration (equation (8)).

$$Mg/Ca = 0.12 \pm 0.01 \times BWT + 1.2 \pm 0.1 \quad (8)$$

Tisserand et al. [2013] present *O. umbonatus* Mg/Ca from oxidatively cleaned core top samples from the saturated thermocline waters of the Brazilian Margin. These samples span a narrow temperature range of ~4 to 6°C, but are useful to consider in the context of other core top data.

For our down core records we avoided deep water sites (>3 km) to maximize the buffering potential of the carbonate sediments (deep water sites tend to contain fewer of the least dissolution-resistant planktonic foraminiferal tests). We take a similar approach with the calibration samples, resulting in an alternative *O. umbonatus*

Table 1. Constants for the Generic Exponential Mg/Ca-Temperature-Mg/Ca_{sw} Calibration (Equation (2)) Calculated by Reconciling the Core Top NS-LBB Exponential and *Lear et al.* [2002] Mg/Ca Temperature Calibrations With the Paleocene-Eocene Record (Figure 4)[a]

	Mg/Ca_{sw} at 52–57 Ma = 1.0		Mg/Ca_{sw} at 52–57 Ma = 1.3		Mg/Ca_{sw} at 52–57 Ma = 2.5	
	A	*H*	*A*	*H*	*A*	*H*
NS-LBB	1.38	0.02	1.37	0.03	1.32	0.05
B = 0.0548	±0.03	±0.01	±0.03	±0.01	±0.06	±0.03
Lear et al. [2002]	0.70	0.23	0.66	0.27	0.46	0.51
B = 0.114	±0.03	±0.03	±0.04	±0.03	±0.05	±0.07

[a]The constants are calculated assuming three different values of Paleocene-Eocene Mg/Ca_{sw}. The value and errors represent the mean and standard error of the constant as determined individually from each of the 12 Paleocene-Eocene samples.

Mg/Ca temperature calibration using a subset ($n = 11$) of the published core top data from two localities. First, we use the shallowest samples from the Norwegian Sea (NS) data set of *Lear et al.* [2010], with bottom water $\Delta CO_3^{2-} > 25$ μmol/kg. Second, we use the samples from the well-saturated waters of the Little Bahama Banks (LBB) data set [*Lear et al.*, 2002], excluding one obvious outlier (Table S3 in the supporting information). We thus maximize the temperature range of the core top calibration data set (−0.8 to 9.9°C), while minimizing the influence of carbonate ion effects. The resulting Mg/Ca temperature relationship can be cast as an exponential or linear equation (equations (9) and (10)), referred to as "NS-LBB-exp" and "NS-LBB-lin," respectively. However, we add a note of caution: as with *O. umbonatus* Li/Ca, *O. umbonatus* Mg/Ca decreases slightly with increasing water depth in the Norwegian Sea (average *O. umbonatus* Mg/Ca from depths >3 km is 0.13 mmol/mol less than average *O. umbonatus* Mg/Ca from depths <3 km) [*Lear and Rosenthal*, 2006; *Lear et al.*, 2010], perhaps suggesting a limit to the buffering capacity of clay-rich sediments.

$$Mg/Ca = 1.43 \pm 0.1 \times \exp(0.055 \pm 0.01 \times BWT)\ r^2 = 0.9 \quad (9)$$

$$Mg/Ca = 1.45 \pm 0.1 + 0.10 \pm 0.02 \times BWT\ r^2 = 0.9 \quad (10)$$

We calculate the constants in equations (2) and (3) for four of these seven calibrations, using the ODP Site 690 Paleocene-Eocene data (Tables 1 and 2). We chose not to use the two *Healey et al.* [2008] calibrations which are useful for the recent deep ocean environment but not appropriate for records from shallower sites. We also did not use the *Rathmann et al.* [2004] calibration, because it may not be appropriate to compare the laser-ablation-based calibration to the solution-based ODP Site 690 record. We therefore use the Mg/Ca temperature calibrations of *Lear et al.* [2002], *Lear et al.* [2010], NS-LBB-lin, and NS-LBB-exp.

In calculating the constants in equations (2) and (3), the temperature variable is relatively well constrained because the modern calibrations are based on measured temperatures, and we use interpolated $\delta^{18}O$ measurements from ODP Site 690 for the Paleocene-Eocene data set, assuming ice-free conditions (section 2.3, Figure 4). We adjust the 690 Mg/Ca record by −9.1% to account for the different cleaning technique relative to the core top samples [*Yu et al.*, 2007]. Echinoderm Mg/Ca ratios have been used to estimate Mg/Ca_{sw} at 53 Ma as 1.7 mol/mol [*Dickson*, 2002], although subsequent reinterpretation of these data using a power law dependency has revised this to 1.3 mol/mol [*Hasiuk and Lohmann*, 2010]. Our calculations assume that

Table 2. Constants for the Generic Linear Mg/Ca-Temperature-Mg/Ca_{sw} Calibration (Equation (3)) Calculated by Reconciling the Core Top NS-LBB Linear and *Lear et al.* [2010] Mg/Ca Temperature Calibrations With the Paleocene-Eocene Record (Figure 4)[a]

	SW Mg/Ca = 1.0			SW Mg/Ca = 1.3			SW Mg/Ca = 2.5		
	m	*c*	*H*	*m*	*c*	*H*	*m*	*c*	*H*
NS-LBB linear	0.098	1.47	−0.007	0.098	1.47	−0.009	0.099	1.49	−0.016
	±0.001	±0.03	±0.01	±0.002	±0.03	±0.01	±0.001	±0.03	±0.02
Lear et al. [2010]	0.121	1.21	−0.003	0.121	1.21	−0.003	0.121	1.21	−0.006
	±0.002	±0.02	±0.01	±0.002	±0.02	±0.012	±0.002	±0.02	±0.02

[a]The constants are calculated assuming three different values of Paleocene-Eocene Mg/Ca_{sw}. The value and errors represent the mean and standard error of the constant as determined individually from each of the 12 Paleocene-Eocene samples.

seawater Mg/Ca was invariant over the duration of the Paleocene-Eocene data set; we compensate for this simplification by using a range of Paleocene-Eocene Mg/Ca_{sw} of 1.0, 1.3, and 2.5 mol/mol to calculate the constants in equations (2) and (3) (Tables 1 and 2). We also calculated the calibration constants after omitting the oldest data point described above (57.1 Ma). The values are within the error of the constants presented in Tables 1 and 2 and are provided in the supporting information.

Using the *Lear et al*. [2002] Mg/Ca temperature calibration, an *H* value of 0.2–0.5 is predicted, depending on the assumed value of Mg/Ca_{sw} in the Paleocene-Eocene (Table 1). Reconciling the Mg/Ca temperature sensitivities of the NS-LBB-exp, NS-LBB-lin and the *Lear et al*. [2010] calibration with our Paleocene-Eocene data set requires *O. umbonatus* to be more or less insensitive to Mg/Ca_{sw} ($H \approx 0$). This would suggest that this deep ocean, low-Mg calcite foraminifer has an effective strategy for controlling the Mg^{2+} concentration at the site of biomineralization, such that test Mg/Ca is only weakly related to Mg/Ca_{sw}. While there is a range of potential biomineralization processes that may influence test Mg/Ca, the exact mechanism remains unknown [*Erez*, 2003; *Dawber and Tripati*, 2012; *Nehrke et al*., 2013; *Mewes et al*., 2014]. Further study is required to test this finding, but if $H = 0$, the Paleocene-Eocene data can be combined with the core top data to extend the Mg/Ca temperature calibration into warmer waters and better constrain the Mg/Ca temperature sensitivity (Figure 4d). The *O. umbonatus* Mg/Ca data from the Brazilian Margin are compatible with this relationship [*Tisserand et al*., 2013] (Figure S2). A compilation of the NS-LBB calibration data with the ODP Site 690 data can be fit equally well with an exponential (equation (11)) or linear (equation (12)) relation. The slope of the linear fit is within the error of a previous calibration based on core top *O. umbonatus* and *C. pachyderma* [*Lear et al*., 2010]. Stated errors in equations (11) and (12) have 95% confidence intervals.

$$\mathrm{Mg/Ca} = 1.44 \pm 0.05 \exp(0.050 \pm 0.005 \times \mathrm{BWT})\ r^2 = 0.94 \quad (11)$$

$$\mathrm{Mg/Ca} = 1.46 \pm 0.09 + 0.10 \pm 0.01 \times \mathrm{BWT}\ r^2 = 0.95 \quad (12)$$

If future work confirms the insensitivity of *O. umbonatus* Mg/Ca to Mg/Ca_{sw}, this paleothermometer could be applied with more confidence to questions of long-term (multi-Myr) climate change.

4.2. ODP Site 806 Versus ODP Site 761: Impact of Porewater Chemistry on Foraminiferal Geochemistry

Mg/Ca values from *O. umbonatus* from the middle Miocene at ODP Site 761 (Wombat Plateau; Figure 3) [*Lear et al*., 2010] are ~0.4 mmol/mol higher than those of time-equivalent samples at ODP Site 806 (Ontong Java Plateau). The magnitude of this offset is somewhat puzzling, given the similarity in $\delta^{18}O$ between the two sites (Figure 3). We consider two possibilities to explain this offset. One possibility is that the higher Mg/Ca at Site 761 is caused by diagenetic carbonate overgrowth. The low sedimentation rates at this site (~0.3 cm/kyr, compared to ~2.5 cm/kyr at ODP Site 806) may have favored the formation of Mn carbonate coatings [*Jarvis et al*., 2001]. Measured Mn/Ca typically falls between 100 and 200 μmol/mol at Site 761, compared to 0–100 μmol/mol at ODP Site 806. However, the Site 761 Mn/Ca record shows an overall increase across the MMCT, whereas the Mg/Ca shows an overall decrease (Figure S3). This does not rule out a diagenetic contribution per se, because the influence of the coatings would be imprinted onto an unknown primary signal, but it makes it more unlikely. Mn can exist in different mineral phases (e.g., different Mn oxide minerals, Mn adsorbed onto calcite, Ca-Mn carbonates, or Mn-Ca-Mg carbonates) [*Boyle*, 1983]. Therefore, samples with Mn/Ca below the proposed threshold of 100 μmol/mol [*Boyle*, 1983] may be considered free of Mn-related contamination, but it is not necessarily true that all samples with Mn/Ca above this threshold are contaminated with respect to Mg/Ca. Pacific ODP Site 1218 provides an example of a site with significant foraminiferal Mn contamination. The ODP Site 1218 record from 20 to 40 Ma displays large variations in Mn/Ca values in reductively cleaned foraminifera, from $<$100 μmol/mol to $>$1000 μmol/mol (Figure S4). Despite this order of magnitude variation in Mn content, there is no relationship between the Mn/Ca and Mg/Ca records, and the highest Mn/Ca values are associated with the lowest Mg/Ca ratios. However, the origin of the Mn at Site 1218 is likely different from that at Site 761. Authigenic $(Mn_x,Mg_y)CaCO_3$ coatings on Pleistocene foraminifera at Caribbean Site 999 resulted in measured Mn/Ca similar to those observed at Site 761 ($<$500 μmol/mol) [*Schmidt et al*., 2006]. Assuming a 10:1 Mn/Mg molar ratio of the authigenic carbonates, the authors demonstrate that less than 0.05 mmol/mol of their measured Mg/Ca could originate from such coatings. Even if we arbitrarily assume a tenfold Mg enrichment in the authigenic carbonate relative to that observed in the Panama Basin [*Pedersen and Price*, 1982], the Mn coatings could not account for more than 0.2 mmol/mol of the

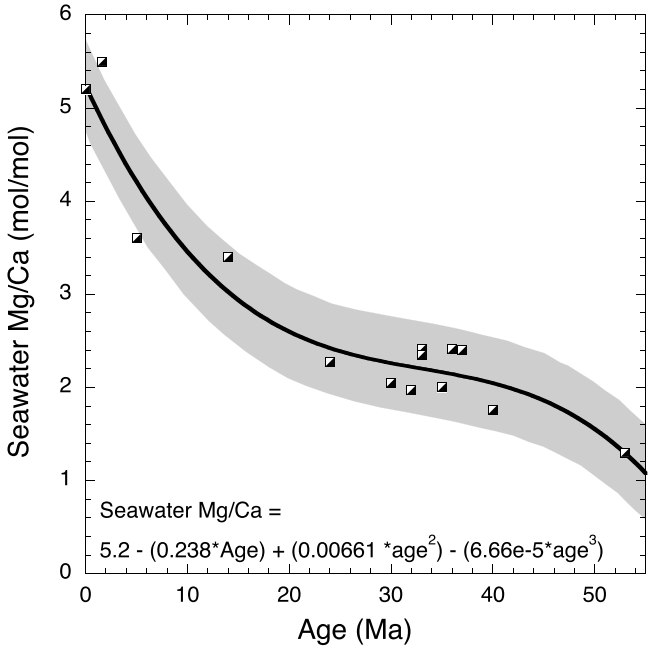

Figure 5. Third-order polynomial curve fit through compiled seawater Mg/Ca proxy records based on fluid inclusions, calcite veins, and echinoderms [*Dickson*, 2002; *Horita et al*., 2002; *Coggon et al*., 2010]. The grey envelope represents the ±0.5 mol/mol uncertainty window used in our temperature calculations.

measured Mg/Ca. We note that there is no offset in *C. mundulus* $\delta^{13}C$ between ODP Sites 806 and 761 (Figure S5). We, therefore, discount this explanation for the intersite offset in Mg/Ca.

The second and favored explanation for the Mg/Ca offset between the two sites is that ODP Site 761 had anomalously high levels of pore water carbonate saturation in which the infaunal *O. umbonatus* precipitated its test calcite. The ODP Site 761 *O. umbonatus* B/Ca values are on average 12 μmol/mol higher than values at ODP Site 806, are more variable, and display a slight increase across the MMCT, whereas the ODP Site 806 B/Ca values are lower and relatively constant (Figure 3). This is consistent with the hypothesis that ODP Site 761 pore waters have a higher degree of carbonate saturation than those at ODP Site 806 [*Yu and Elderfield*, 2007]. A core top study estimated *O. umbonatus* Mg/Ca and B/Ca sensitivity to ΔCO_3^{2-} as 0.0164 mmol/mol/μmol/kg and 0.433 μmol/mol/μmol/kg, respectively [*Dawber and Tripati*, 2012]; *Brown et al*. [2011] estimated *O. umbonatus* B/Ca-ΔCO_3^{2-} sensitivity as 0.29 ± 0.20 μmol/mol/μmol/kg. It is not straightforward to interpret these sensitivities directly in terms of changes in bottom water versus pore water saturation states. Nevertheless, if the *O. umbonatus* 0.4 mmol/mol Mg/Ca offset between ODP Sites 806 and 761 is caused solely by an offset in ΔCO_3^{2-}, one would expect a corresponding offset in B/Ca ~11 μmol/mol, in excellent agreement with our record (Figure 3). However, we do not observe an intersite offset in *O. umbonatus* Sr/Ca, and the observed intersite offset in *O. umbonatus* Li/Ca is twice the expected magnitude, albeit in the expected direction (higher Li/Ca at ODP Site 761). This may point to uncertainties in core top ΔCO_3^{2-} calibrations, or additional, unknown processes at work.

The reasons for the hypothesized increased pore water saturation state at ODP Site 761 are unknown. However, we note that the pore water [Mg] and [Ca] profiles at this site are atypical for pelagic marine sediments, in that their concentrations remain relatively constant from the sea floor down to ~300 m below seafloor [*De Carlo*, 1992]. As the organic carbon content of the sediment is low, these trends are unlikely to be caused by enhanced dissolution due to remineralization of organic matter. Instead, these profiles may reflect unusual flushing of the sediments by (oversaturated) seawater, perhaps aided by the unusually low sedimentation rates [*De Carlo*, 1992]. Hence, it is plausible that the ODP Site 761 Mg/Ca might be biased by the unusual pore water chemistry at the site.

4.3. Estimating Neogene BWT and $\delta^{18}O_{sw}$

We use our calibration equations (Tables 1 and 2) and a record of Mg/Ca_{sw} from fluid inclusion, calcite vein and echinoderm proxies [*Dickson*, 2002; *Horita et al*., 2002; *Coggon et al*., 2010] to calculate absolute BWT from our ODP Site 806 Mg/Ca record. We fit a third-order polynomial curve through the compiled Mg/Ca_{sw} data and use an uncertainty window of ±0.5 mol/mol to encompass most of the proxy data (Figure 5). Each BWT scenario is then used in conjunction with the $\delta^{18}O$ record from the same samples and the *Cibicidoides* quadratic $\delta^{18}O$ paleotemperature equation of *Marchitto et al*. [2014] to calculate $\delta^{18}O_{sw}$. The result is a suite of alternative calculated records for the evolution of deep Pacific bottom water temperature and $\delta^{18}O_{sw}$ since 17 Ma (Figure 6). The range in predicted temperature and $\delta^{18}O_{sw}$ results from a combination of the following:

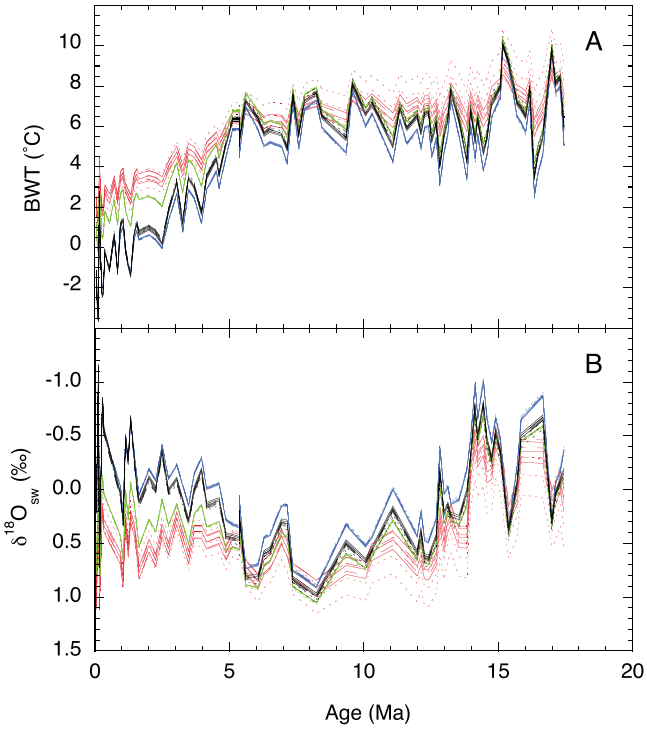

Figure 6. (a) Absolute bottom water temperature and (b) seawater $\delta^{18}O$ scenarios using the equations in Tables 1 and 2. Equations based on *Lear et al*. [2002] are shown in red, on *Lear et al*. [2010] in green, the NS-LBB linear calibration in blue, and the NS-LBB exponential calibration in black. Scenarios that assume early Eocene seawater Mg/Ca = 1.0 are marked by long dashes, seawater Mg/Ca = 1.3 by solid lines, and seawater Mg/Ca = 2.5 by dotted line.

(1) differences between Mg/Ca temperature calibrations, (2) the 1.0–2.5 mol/mol range of assumed Paleocene-Eocene Mg/Ca_{sw} used to calculate the constants in Tables 1 and 2, and (3) the ±0.5 mol/mol envelope on the Mg/Ca_{sw} curve (Figure 5). Refining the Mg/Ca temperature calibration is key to improving estimates of absolute temperature and $\delta^{18}O_{sw}$ over long (Myr) timescales (Figure 6). The Pleistocene portion of our record is at too low a resolution to capture the amplitude of glacial-interglacial cycles. Based on the expected range of Pleistocene $\delta^{18}O_{sw}$ [*Duplessy et al*., 2002; *Elderfield et al*., 2012], our preferred linear Mg/Ca temperature calibration is that of *Lear et al*. [2010] and our preferred exponential Mg/Ca temperature calibration is that of *Lear et al*. [2002] (Figure 6). We show the full range of absolute BWT and $\delta^{18}O$ estimates based on these two calibrations (Figure 7). The uncertainty window on these absolute estimates results from the set of constants corresponding to the 1.0–2.5 mol/mol range assumed for late Paleocene seawater Mg/Ca (Tables 1 and 2) and the ±0.5 mol/mol envelope on the Neogene Mg/Ca_{sw} curve (Figure 5). After calculating the maximum and minimum temperatures produced from different combinations of these parameters through time, an additional ±1°C uncertainty envelope was added to the record to include sample reproducibility and calibration errors [*Elderfield et al*., 2012].

4.4. Neogene Ice Sheet Evolution and Ocean Cooling

The low-resolution $\delta^{18}O$ and Mg/Ca records from ODP Site 806 (Figure 2) capture the broad trends in late Neogene Pacific deep water temperature and $\delta^{18}O_{sw}$ (Figure 7). The records display three noteworthy features, which we discuss in more detail below. First, bottom waters cooled between 15.5 and 14.5 Ma (following the Miocene Climatic Optimum), but there was apparently no significant cooling associated with major ice growth steps between 14 and 12 Ma. Second, $\delta^{18}O_{sw}$ has increased by ~0.5‰ overall since ~15 Ma (prior to the MMCT), with an interval of heavy $\delta^{18}O_{sw}$ between 12 and 8 Ma that could be interpreted as reflecting bipolar glaciation or the presence of a relatively warm salty water mass at Site 806. We acknowledge that these absolute estimates of $\delta^{18}O_{sw}$ are poorly constrained. Improved core top calibrations will significantly reduce the uncertainties (Figure 6). The third feature is the major deep water cooling since 5 Ma. The Plio-Pleistocene drop in sea level is likely within the uncertainty of this broad reconstruction and cannot be inferred from this low-resolution record.

4.4.1. Neogene Decoupling of Deep Water Temperature and Ice Volume

The decoupling of deep water/high-latitude temperature and ice volume appears to be a consistent feature throughout the late Neogene (Figure 7). This supports our understanding of the cryosphere as a highly thresholded system, with ice growth occurring once the balance between ice accumulation and ablation is favorable [*DeConto et al*., 2008].

4.4.2. Greater than Modern Ice Volume Following the MMCT

Assuming that the $\delta^{18}O_{sw}$ signal can be interpreted in terms of global ice volume, our record suggests greater than modern ice volume following the Middle Miocene Climate Transition. The Pleistocene $\delta^{18}O_{sw}$-sea level

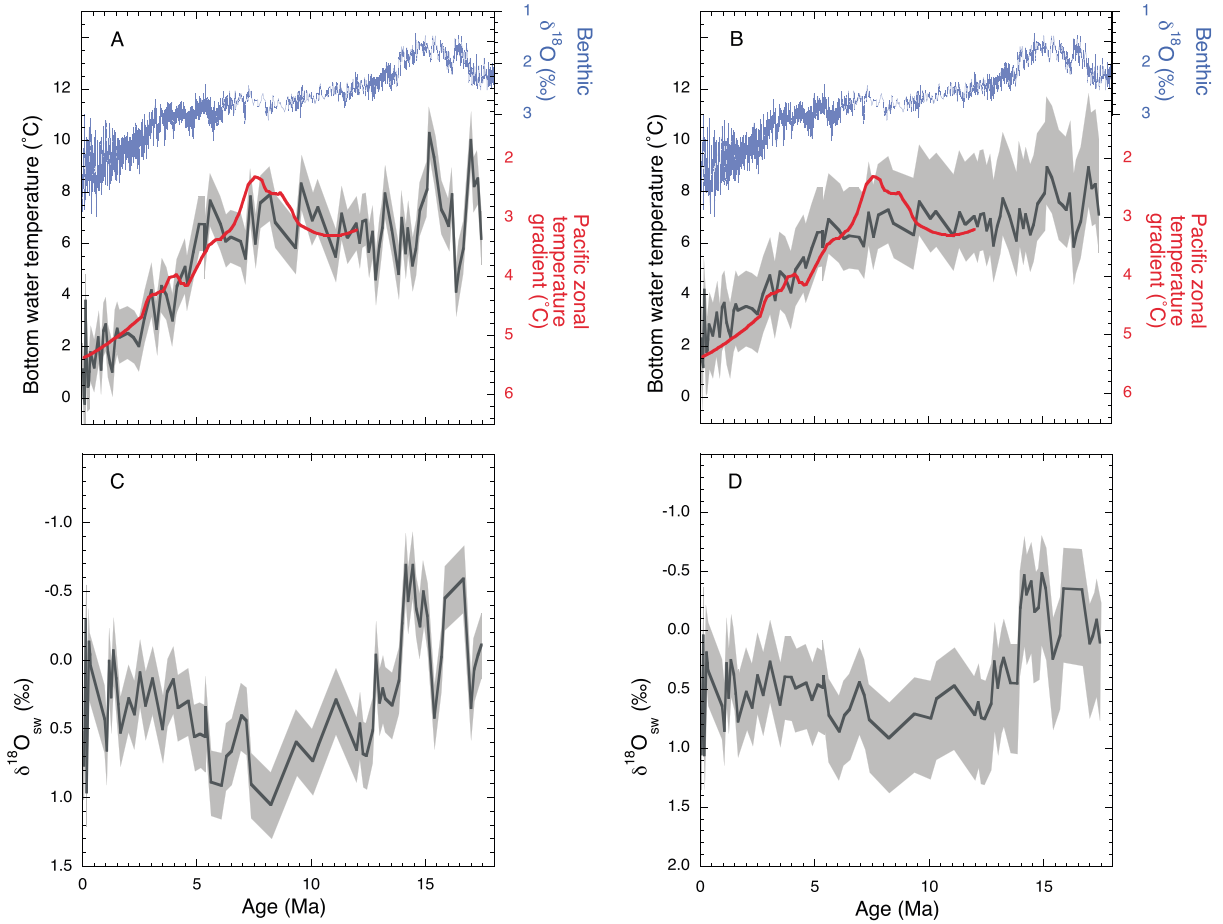

Figure 7. (a, b) Absolute estimates of bottom water temperature and (c, d) seawater $\delta^{18}O$ for ODP Site 806 calculated using the equation based on the *Lear et al.* [2010] calibration (Figures 7a and 7c) and the equation based on the *Lear et al.* [2002] calibration (Figures 7b and 7d). The uncertainty envelope is derived from the range in calibration constants in Tables 1 and 2, the range in seawater Mg/Ca shown by the grey envelope in Figure 5 and a further ±1°C uncertainty to reflect sample reproducibility and calibration error. The solid grey lines represent our favored scenarios, which assume Paleocene-Eocene seawater Mg/Ca =1.3 and use values for Neogene seawater Mg/Ca shown by the solid black line in Figure 5. These records assume constant pore water saturation state. The Pacific zonal sea surface temperature gradient (red line, Figures 7a and 7b) has been calculated from TEX_{86} records [*Zhang et al.*, 2014], and the benthic $\delta^{18}O$ record (blue line) was compiled by *Zachos et al.* [2008].

calibration [*Fairbanks and Matthews*, 1978] indicates that the ~1‰ increase in $\delta^{18}O_{sw}$ between 14.5 and 12.5 Ma is equivalent to a ~90 m sea level fall. Put into context, the modern Antarctic ice sheet contains approximately 60 m sea level equivalent ice, and during the Last Glacial Maximum (LGM), sea levels were approximately 120 m lower than today, with around ~14 m attributed to a larger Antarctic ice sheet [*Denton and Hughes*, 2002; *Briggs et al.*, 2014]. The amount of ice that can be supported on Antarctica depends not only on climate parameters but also on paleotopography and paleogeography. Drilling off the East Antarctic coast has revealed a dynamic Miocene history for the Antarctic ice sheet [*Escutia et al.*, 2005; *Passchier et al.*, 2011]. Age model uncertainties prevent us from correlating intervals of East Antarctic ice sheet advance to our $\delta^{18}O_{sw}$ records, but diamictite textures indicating offshore grounding lines provide evidence for a greater ice sheet extent than today during the middle Miocene [*Passchier et al.*, 2011]. Paleogeographic reconstructions demonstrate that Antarctic land area has decreased since the earliest Oligocene, with early Oligocene climate and topography supporting an Antarctic ice sheet ~35% larger than today [*Wilson et al.*, 2013]. Furthermore, geomorphological evidence indicates that a thicker-than-modern ice sheet, capable of cross-cutting valleys, overrode the Transantarctic Mountains in the middle Miocene [*Denton et al.*, 1984; *Denton and Sugden*, 2005]. These lines of evidence suggest that Middle Miocene Antarctic paleogeography and climate were able to support a far larger ice sheet than today. However, it is surprising that the high absolute $\delta^{18}O_{sw}$ values persisted and even slightly increased throughout the late Miocene (Figure 7).

We consider two explanations for this unexpected finding. The first is that there was a period of significant Northern Hemisphere glaciation, culminating around 8 Ma, and the second is that the Site 806 $\delta^{18}O_{sw}$ record includes a significant component of regional salinity change. Middle Miocene paleotopographic reconstructions indicate a high relief (>1500 m) in the northwestern Barents Sea. Ice rafted debris (IRD) fingerprinting has been interpreted in terms of significant glaciation and iceberg calving in the Barents Sea region from ~14 Ma [*Knies and Gaina*, 2008]. Perennial ice has provided a constant source of IRD from all the circum-Arctic shelves since ~15 Ma [*Darby*, 2008], and Scandinavian ice, as inferred from IRD on the Vöring Plateau, initiated around 12.6 Ma [*Thiede et al*., 1998]. Therefore, there may have been a Northern Hemisphere glaciation component following the MMCT, consistent with the hypothesis that atmospheric CO_2 levels crossed the proposed threshold for Northern Hemisphere glaciation at the Middle Miocene Climate Transition [*Foster et al*., 2012; *DeConto et al*., 2008; *Holbourn et al*., 2013a]. However, evidence for extensive Northern Hemisphere continental ice sheets prior to ~7 Ma is lacking [*Larsen et al*., 1994].

Alternatively, our Site 806 $\delta^{18}O_{sw}$ record includes a significant regional salinity signal. In the middle Miocene, ODP Site 806 likely lay in the path of Pacific Central Water, the return flow of Circumpolar Deep Water [*Holbourn et al*., 2013b]. Intersite stable isotope gradients indicate enhanced formation of North Atlantic Deep Water (NADW) during the early Pliocene relative to today, and this relatively warm, salty water mass may have influenced deep Pacific waters [*Kwiek and Ravelo*, 1999; *Ravelo and Andreasen*, 2000]. Closure of the Tethys Seaway may have increased Atlantic sea surface salinity and promoted enhanced formation of NADW since the middle Miocene, with consequent cooling of the Southern Ocean [*Zhang et al*., 2011] and an increased NADW influence on Circumpolar Deep Water [*Holbourn et al*., 2013b]. We note that the upper Miocene benthic foraminiferal $\delta^{18}O$ record from ODP Site 806 appears to diverge from the compiled adjusted $\delta^{18}O$ record of abyssal Pacific Deep Sea Drilling Project Site 77 (paleowater depth ~4 km [*Cramer et al*., 2009] (Figure S6). We speculate that warmer, saltier waters bathed ODP Site 806, while the Pacific abyss was bathed by a fresher, colder water mass sourced from high latitudes. High-resolution quantitative reconstructions of $\delta^{18}O_{sw}$ from different ocean basins are required to tease out the global ice volume and regional salinity components of the Site 806 $\delta^{18}O_{sw}$ record and hence the link between climate sensitivity and ocean overturning regime.

4.4.3. Plio-Pleistocene Deep Water Cooling

Our records display a striking cooling trend of ~4–6°C from around 5 Ma to ~2.5 Ma, preceding the onset of large-amplitude glacial-interglacial cycles in the late Pliocene [*Raymo et al*., 1989; *Bailey et al*., 2013] (Figure 7). The later half of this trend corresponds to a sea surface cooling linked to increased iceberg longevity in the Southern Ocean [*Cook et al*., 2014]. However, the early phase (between 5 and 4 Ma) of bottom water cooling at Site 806 does not appear to be associated with significant cooling in the Southern Ocean. This cooling might reflect increasing dominance of a cold water mass, rather than a cooling in its source region. In the early Pliocene, north Pacific ODP Site 1018 (2476 m water depth) was apparently influenced by a water mass that was warmer and saltier than modern NADW [*Kwiek and Ravelo*, 1999]. We speculate that this water mass also influenced ODP Site 806 but became less important between 5 and 4 Ma. The cooling is paralleled by an increase in the tropical Pacific zonal sea surface temperature gradient (Figure 7), which may have been driven by an increased meridional sea surface temperature gradient [*Zhang et al*., 2014]. The associated thinning of the low-latitude thermocline may have increased climate sensitivity to CO_2, thus setting the stage for the subsequent glaciation of the Northern Hemisphere [*LaRiviere et al*., 2012].

5. Conclusions

Benthic foraminiferal Mg/Ca paleothermometry is a powerful tool for reconstructing bottom water temperatures and $\delta^{18}O_{sw}$. Infaunal foraminifera calcify in pore waters that may be buffered from changes in overlying bottom water saturation state. We recommend that paired B/Ca and Mg/Ca records are used to assess this assumption, before Mg/Ca records are interpreted solely in terms of bottom water temperature. We suggest that sediments with abundant planktonic foraminifera (which dissolve more easily than benthics) may have a higher buffering capacity than sediment without or with rare planktonic foraminifera, and/or a high fragmentation index. Paired Mg/Ca and $\delta^{18}O$ records from the ice-free late Paleocene to early Eocene imply a low sensitivity of *O. umbonatus* Mg/Ca to seawater Mg/Ca, suggesting that this infaunal deep water species exerts a strong biological control on its calcification process. We provide a range of possible Mg/Ca-BWT-Mg/Ca_{sw}

calibrations for calculating absolute BWT and $\delta^{18}O_{sw}$, encompassing uncertainties resulting from core top calibrations and Cenozoic Mg/Ca_{sw} reconstructions. Uncertainties in reconstructed absolute BWT and $\delta^{18}O_{sw}$ are large compared to relative changes in BWT and $\delta^{18}O_{sw}$ as determined over short timescales (<1 Myr). Nevertheless, when applied to an *O. umbonatus* Mg/Ca record from ODP Pacific Site 806, our calibrations imply greater than modern ice volume following the Middle Miocene Climate Transition. Bottom waters at Site 806 cooled in the Pliocene, as meridional and tropical zonal sea surface temperature gradients increased, thus supporting the idea that a change in ocean hydrographic regime played an important role in Earth's transition from a polar to bipolar glaciated world. The apparent decoupling of deep water/high-latitude temperatures and ice volume highlights the sensitivity of the cryosphere to thresholds and internal feedbacks in the climate system.

Acknowledgments

Data from ODP Sites 806 and 690 can be found in Tables S1 and S2 of the supporting information. We thank Huw Boulton, Alexandra Nederbragt, and Anabel Morte-Rodeñas for laboratory assistance. We thank Jim Zachos and an anonymous reviewer for their insightful comments, and Heiko Pälike for efficient editorial handling. This research used samples provided by the Integrated Ocean Drilling Program (IODP) and was supported by NERC grants NE/D000041/1 and NE/I006427/1 (C.H.L.), NE/I006176/1 (G.L.F. and C.H.L.), and NERC studentship NE/F016603/1 (E.M.M.).

References

Bailey, I., G. M. Hole, G. L. Foster, P. A. Wilson, C. D. Storey, C. N. Trueman, and M. E. Raymo (2013), An alternative suggestion for the Pliocene onset of major Northern Hemisphere glaciation based on the geochemical provenance of North Atlantic Ocean ice-rafted debris, *Quat. Sci. Rev.*, *75*, 181–194.

Barker, P. E., et al. (1988), *Proceedings of the Ocean Drilling Program*, *Initial Rep.*, vol. 113, Ocean Drill. Program, College Station, Tex., doi:10.2973/odp.proc.ir.113.1988.

Billups, K., and D. P. Schrag (2002), Paleotemperatures and ice volume of the past 27 Myr revisited with paired Mg/Ca and $^{18}O/^{16}O$ measurements on benthic foraminifera, *Paleoceanography*, *17*(1), 1003, doi:10.1029/2000PA000567.

Billups, K., and D. P. Schrag (2003), Application of benthic foraminiferal Mg/Ca ratios to questions of Cenozoic climate change, *Earth Planet. Sci. Lett.*, *209*, 181–195.

Bohaty, S. M., J. C. Zachos, and M. L. Delaney (2012), Foraminiferal Mg/Ca evidence for Southern Ocean cooling across the Eocene-Oligocene transition, *Earth Planet. Sci. Lett.*, *317-318*, 251–261.

Boyle, E. A. (1983), Manganese carbonate overgrowths on foraminifera tests, *Geochim. Cosmochim. Acta*, *47*, 1815–1819.

Boyle, E. A., and L. D. Keigwin (1985), Comparison of Atlantic and Pacific paleochemical records for the last 250,000 years: Changes in deep ocean circulation and chemical inventories, *Earth Planet. Sci. Lett.*, *76*, 135–150.

Briggs, R. D., D. Pollard, and L. Tarasov (2014), A data-constrained large ensemble analysis of Antarctic evolution since the Eemian, *Quat. Sci. Rev.*, *103*, 91–115.

Broecker, W. S., and T.-H. Peng (1982), *Tracers in the Sea*, Eldigo, Palisades, New York.

Brown, R. E., L. D. Anderson, E. Thomas, and J. C. Zachos (2011), A core-top calibration of B/Ca in the benthic foraminifers *Nuttallides umbonifera* and *Oridorsalis umbonatus*: A proxy for Cenozoic bottom water carbonate saturation, *Earth Planet. Sci. Lett.*, *241*, 360–368.

Coggon, R. M., D. A. H. Teagle, C. E. Smith-Duque, J. C. Alt, and M. J. Cooper (2010), Reconstructing past seawater Mg/Ca and Sr/Ca from mid-ocean ridge flank calcium carbonate veins, *Science*, *327*, 1114–1117, doi:10.1126/science.1182252.

Cook, C. P., et al. (2014), Sea surface temperature control on the distribution of far-traveled Southern Ocean ice-rafted detritus during the Pliocene, *Paleoceanography*, *29*, 533–548, doi:10.1002/2014PA002625.

Coxall, H. K., P. A. Wilson, H. Pälike, C. H. Lear, and J. Backman (2005), Rapid stepwise onset of Antarctic glaciation and deeper calcite compensation in the Pacific Ocean, *Nature*, *433*, 53–57.

Cramer, B. S., J. R. Toggweiler, J. D. Wright, M. E. Katz, and K. G. Miller (2009), Ocean overturning since the Late Cretaceous: Inferences from a new benthic foraminiferal isotope compilation, *Paleoceanography*, *24*, PA4216, doi:10.1029/2008PA001683.

Cramer, B. S., K. G. Miller, P. J. Barrett, and J. D. Wright (2011), Late Cretaceous-Neogene trends in deep ocean temperature and continental ice volume: Reconciling records of benthic foraminiferal geochemistry ($\delta^{18}O$ and Mg/Ca) with sea level history, *J. Geophys. Res.*, *116*, C12023, doi:10.1029/2011JC007255.

Darby, D. A. (2008), Arctic perennial ice cover over the last 14 million years, *Paleoceanography*, *23*, PA1S07, doi:10.1029/2007PA001479.

Dawber, C. F., and A. Tripati (2012), Relationships between bottom water carbonate saturation and element/Ca ratios in coretop samples of the benthic foraminifera *Oridorsalis umbonatus*, *Biogeosciences*, *9*, 3029–3045.

De Carlo, E. H. (1992), Geochemistry of pore water and sediments recovered from the Exmouth Plateau, in *Proceedings of the Ocean Drilling Program*, *Sci. Results*, vol. 122, pp. 295–308, Ocean Drilling Program, College Station, Tex.

DeConto, R. M., D. Pollard, P. A. Wilson, H. Pälike, C. H. Lear, and M. Pagani (2008), Thresholds for Cenozoic bipolar glaciation, *Nature*, *455*, 652–656, doi:10.1038/nature07337.

Delaney, M. L., A. W. H. Bé, and E. A. Boyle (1985), Li, Sr, Mg, and Na in foraminiferal calcite shells from laboratory culture, sediment traps, and sediment cores, *Geochim. Cosmochim. Acta*, *49*, 1327–1341.

Denton, G. H., and T. J. Hughes (2002), Reconstructing the Antarctic ice sheet at the Last Glacial Maximum, *Quat. Sci. Rev.*, *21*, 193–202.

Denton, G. H., and D. E. Sugden (2005), Meltwater features that suggest Miocene ice-sheet overriding of the Transantarctic Mountains in Victoria Land, Antarctica, *Geogr. Ann., Ser. A*, *87*(1), 67–85.

Denton, G. H., M. L. Prentice, D. E. Kellogg, and T. B. Kellogg (1984), Late Tertiary history of the Antarctic ice sheet: Evidence from the Dry Valleys, *Geology*, *12*, 263–267.

Dickson, J. A. D. (2002), Fossil echinoderms as monitor of the Mg/Ca ratio of Phanerozoic Oceans, *Science*, *298*, 1222–1224.

Duplessy, J.-C., L. Labeyrie, and C. Waelbroeck (2002), Constraints on the ocean oxygen isotopic enrichment between the Last Glacial Maximum and the Holocene: Paleoceanographic implications, *Quat. Sci. Rev.*, *21*, 315–330.

Edgar, K. M., P. A. Wilson, P. F. Sexton, and Y. Suganuma (2007), No extreme bipolar glaciation during the main Eocene calcite compensation shift, *Nature*, *448*, 908–911, doi:10.1038/nature06053.

Edgar, K. M., H. Pälike, and P. A. Wilson (2013), Testing the impact of diagenesis on the $\delta^{18}O$ and $\delta^{13}C$ of benthic foraminiferal calcite from a sediment burial depth transect in the equatorial Pacific, *Paleoceanography*, *28*, 468–480, doi:10.1002/palo.20045.

Elderfield, H., J. Yu, P. Anand, T. Kiefer, and B. Nyland (2006), Calibrations for benthic foraminiferal Mg/Ca paleothermometry and the carbonate ion hypothesis, *Earth Planet. Sci. Lett.*, *250*, 633–649.

Elderfield, H., M. Greaves, S. Barker, I. R. Hall, A. Tripati, P. Ferretti, S. Crowhurst, L. Booth, and C. Daunt (2010), A record of bottom water temperature and seawater $\delta^{18}O$ for the Southern Ocean over the past 440 kyr based on Mg/Ca of benthic foraminiferal Uvigerina spp, *Quat. Sci. Rev.*, *29*, 160–169, doi:10.1016/j.quascirev.2009.07.013.

Elderfield, H., P. Ferretti, M. Greaves, S. Crowhurst, I. N. McCave, D. Hodell, and A. M. Piotrowski (2012), Evolution of ocean temperature and ice volume through the mid-Pleistocene climate transition, *Science*, *337*, 704–709.
Eldrett, J. S., I. C. Harding, P. A. Wilson, E. Butler, and A. P. Roberts (2007), Continental ice in Greenland during the Eocene and Oligocene, *Nature*, *446*, 176–179.
Erez, J. (2003), The source of ions for biomineralization in foraminifera and their implications for paleoceanographic proxies, *Rev. Mineral. Geochem.*, *54*, 115–149.
Escutia, C., L. D. De Santis, F. Donda, R. B. Dunbar, A. K. Cooper, G. Brancolini, and S. L. Eittreim (2005), Cenozoic ice sheet history from East Antarctic Wilkes Land continental margin sediments, *Global Planet. Change*, *45*, 51–81.
Evans, D., and W. Müller (2012), Deep time foraminifera Mg/Ca paleothermometry: Nonlinear correction for secular change in seawater Mg/Ca, *Paleoceanography*, *27*, PA4205, doi:10.1029/2012PA002315.
Fairbanks, R. G., and R. K. Matthews (1978), The marine oxygen isotope record in Pleistocene coral, Barbados, West Indies, *Quat. Res.*, *10*, 181–196, doi:10.1016/0033-5894(78)90100-X.
Foster, G. L., C. H. Lear, and J. W. B. Rae (2012), The evolution of pCO_2, ice volume and climate during the middle Miocene, *Earth Planet. Sci. Lett.*, *341*, 243–254, doi:10.1016/j.epsl.2012.06.007.
Foster, L. C., D. N. Schmidt, E. Thomas, S. Arndt, and A. Ridgwell (2013), Surviving rapid climate change in the deep-sea during the Paleogene hyperthermals, *Proc. Natl. Acad. Sci. U.S.A.*, *110*, 9273–9276.
Hasiuk, F. J., and K. C. Lohmann (2010), Application of calcite Mg partitioning functions to the reconstruction of paleocean Mg/Ca, *Geochim. Cosmochim. Acta*, *74*, 6751–6763.
Healey, S. L., R. C. Thunell, and B. H. Corliss (2008), The Mg/Ca-temperature relationship of benthic foraminiferal calcite: New core-top calibrations in the <4 °C temperature range, *Earth Planet. Sci. Lett.*, *272*, 523–530.
Holbourn, A., W. Kuhnt, M. Schulz, and H. Erlenkeuser (2005), Impacts of orbital forcing and atmospheric carbon dioxide on Miocene ice-sheet expansion, *Nature*, *438*, 483–487.
Holbourn, A., W. Kuhnt, M. Schulz, J. Flores, and N. Anderson (2007), Orbitally paced climate evolution during the middle Miocene "Monterey" carbon isotope excursion, *Earth Planet. Sci. Lett.*, *261*, 534–550.
Holbourn, A., W. Kuhnt, S. Clemens, W. Prell, and N. Andersen (2013a), Middle to late Miocene stepwise climate cooling: Evidence from a high-resolution deep water isotope curve spanning 8 million years, *Paleoceanography*, *28*, 688–699, doi:10.1002/2013PA002538.
Holbourn, A., W. Kuhnt, M. Frank, and B. A. Haley (2013b), Changes in Pacific Ocean circulation following the Miocene onset of permanent Antarctic ice cover, *Earth Planet. Sci. Lett.*, *365*, 38–50.
Horita, J., H. Zimmermann, and H. D. Holland (2002), Chemical evolution of seawater during the Phanerozoic: Implications from the record of marine evaporites, *Geochim. Cosmochim. Acta*, *66*, 3733–3756.
Jarvis, I., A. M. Murphy, and A. S. Gale (2001), Geochemistry of pelagic and hemipelagic carbonates: Criteria for identifying systems tracts and sea-level change, *J. Geol. Soc. London*, *158*, 685–696.
John, C. M., G. D. Karner, E. Browning, R. M. Leckie, Z. Mateo, B. Carson, and C. Lowery (2011), Timing and magnitude of Miocene eustasy derived from the mixed siliciclastic-carbonate stratigraphic record of the northeastern Australian margin, *Earth Planet. Sci. Lett.*, *304*, 455–467.
Jorissen, F. J., C. Fontanier, and E. Thomas (2007), Paleoceanographical proxies based on deep-sea benthic foraminiferal assemblage characteristics, in *Proxies in Late Cenozoic Paleoceanography: Part 2: Biological Tracers and Biomarkers*, edited by C. Hillaire-Marcel and A. de Vernal, pp. 263–326, Elsevier, Amsterdam.
Katz, M. E., D. R. Katz, J. D. Wright, K. G. Miller, D. K. Pak, N. J. Shackleton, and E. Thomas (2003), Early Cenozoic benthic foraminiferal isotopes: Species reliability and interspecies correction factors, *Paleoceanography*, *18*(2), 1024, doi:10.1029/2002PA000798.
Kelly, D. C., T. M. J. Nielsen, and S. A. Schellenberg (2012), Carbonate saturation dynamics during the Paleocene-Eocene thermal maximum: Bathyal constraints from ODP sites 689 and 690 in the Weddell Sea (Antarctica), *Mar. Geol.*, *303*, 75–86.
Kennett, J. P., and L. D. Stott (1990), Proteus and Proto-Oceanus: Ancestral Paleogene oceans as revealed from Antarctic stable isotopic results: ODP Leg 113, in *Proceedings of the Ocean Drilling Program, Sci. Results*, vol. 113, edited by P. F. Barker et al., pp. 865–880, Ocean Drill. Program, College Station, Tex., doi:10.2973/odp.proc.sr.113.188.1990.
Knies, J., and C. Gaina (2008), Middle Miocene ice sheet expansion in the Arctic: Views from the Barents Sea, *Geochem. Geophys. Geosyst.*, *9*, Q02015, doi:10.1029/2007GC001824.
Kroenke, L. W., et al. (1991), *Proceedings of the Ocean Drilling Program, Initial Rep.*, vol. 130, Ocean Drill. Program, College Station, Tex., doi:10.2973/odp.proc.ir.130.1991.
Kwiek, P. B., and A. C. Ravelo (1999), Pacific Ocean intermediate and deep water circulation during the Pliocene, *Palaeogeogr. Palaeoclimatol. Palaeoecol.*, *154*, 191–217.
LaRiviere, J. P., A. C. Ravelo, A. Crimmins, P. S. Dekens, H. L. Ford, M. Lyle, and M. W. Wara (2012), Late Miocene decoupling of oceanic warmth and atmospheric carbon dioxide forcing, *Nature*, *486*, 97–100.
Larsen, H. C., A. D. Saunders, P. D. Clift, J. Beget, W. Wei, S. Spezzaferri, and ODP Leg 152 Scientific Party (1994), Seven million years of glaciation in Greenland, *Science*, *264*, 952–955.
Lear, C. H., and Y. Rosenthal (2006), Benthic foraminiferal Li/Ca: Insights into Cenozoic seawater carbonate saturation state, *Geology*, *34*, 985–988, doi:10.1130/G22792A.1.
Lear, C. H., H. Elderfield, and P. A. Wilson (2000), Cenozoic deep-sea temperatures and global ice volumes from Mg/Ca in benthic foraminiferal calcite, *Science*, *287*, 269–272.
Lear, C. H., Y. Rosenthal, and N. Slowey (2002), Benthic foraminiferal Mg/Ca-paleothermometry: A revised core-top calibration, *Geochim. Cosmochim. Acta*, *66*, 3375–3387.
Lear, C. H., Y. Rosenthal, and J. D. Wright (2003), The closing of a seaway: Ocean water masses and global climate change, *Earth Planet. Sci. Lett.*, *210*, 425–436.
Lear, C. H., Y. Rosenthal, H. K. Coxall, and P. A. Wilson (2004), Late Eocene to early Miocene ice sheet dynamics and the global carbon cycle, *Paleoceanography*, *19*, PA4015, doi:10.1029/2004PA001039.
Lear, C. H., T. R. Bailey, P. N. Pearson, H. K. Coxall, and Y. Rosenthal (2008), Cooling and ice-growth across the Eocene-Oligocene transition, *Geology*, *36*, 251–254.
Lear, C. H., E. M. Mawbey, and Y. Rosenthal (2010), Cenozoic benthic foraminiferal Mg/Ca and Li/Ca records: Towards unlocking temperatures and saturation states, *Paleoceanography*, *25*, PA4215, doi:10.1029/2009PA001880.
Lewis, A. R., D. R. Marchant, A. C. Ashworth, S. R. Hemming, and M. L. Machlus (2007), Major middle Miocene global climate change: Evidence from East Antarctica and the Transantarctic Mountains, *GSA Bull.*, *119*, 1449–1461, doi:10.1130/0016-7606(2007)119[1449:MMMGCC]2.0.CO;2.

Littler, K., U. Roehl, T. Westerhold, and J. C. Zachos (2014), A high-resolution benthic stable isotope record for the South Atlantic: Implications for orbital scale changes in Late Paleocene–Early Eocene climate and carbon cycling, *Earth Planet. Sci. Lett.*, *401*, 18–30.

Liu, Z., M. Pagani, D. Zinniker, R. DeConto, M. Huber, H. Brinkhuis, S. R. Shah, R. M. Leckie, and A. Pearson (2009), Global cooling during the Eocene-Oligocene transition, *Science*, *323*, 1187–1190.

Lyle, M., et al. (2002), *Proceedings of the Ocean Drilling Program, Initial Rep.*, vol. 199, Ocean Drill. Program, College Station, Tex., doi:10.2973/odp.proc.ir.199.2002.

Marchitto, T. M., S. P. Bryan, W. B. Curry, and D. C. McCorkle (2007), Mg/Ca temperature calibration for the benthic foraminifer *Cibicidoides pachyderma*, *Paleoceanography*, *22*, PA1203, doi:10.1029/2006PA001287.

Marchitto, T. M., W. B. Curry, J. Lynch-Stieglitz, S. P. Bryan, K. M. Cobb, and D. C. Lund (2014), Improved oxygen isotope temperature calibrations for cosmopolitan benthic foraminifera, *Geochim. Cosmochim. Acta*, *130*, 1–11.

Martin, P. A., D. W. Lea, Y. Rosenthal, N. J. Shackleton, M. Sarnthein, and T. Papenfuss (2002), Quaternary deep sea temperature histories derived from benthic foraminiferal Mg/Ca, *Earth Planet. Sci. Lett.*, *198*, 193–209.

Mawbey, E. M., and C. H. Lear (2013), Carbon cycle feedbacks during the Oligocene-Miocene transient glaciation, *Geology*, doi:10.1130/G34422.1.

Mewes, A., G. Langer, L. Jan de Nooijer, J. Bijma, and G.-J. Reichart (2014), Effect of different seawater Mg^{2+} concentrations on calcification in two benthic foraminifers, *Mar. Micropaleontol.*, *113*, 56–64.

Miller, K. G., R. G. Fairbanks, and G. S. Mountain (1987), Tertiary oxygen isotope synthesis, sea-level history, and continental margin erosion, *Paleoceanography*, *2*, 1–19, doi:10.1029/PA002i001p00001.

Mudelsee, M., T. Bickert, C. H. Lear, and G. Lohmann (2014), Cenozoic climate changes: A review based on time series analysis of marine benthic $\delta^{18}O$ records, *Rev. Geophys.*, *52*, 333–374, doi:10.1002/2013RG000440.

Nathan, S. A., and R. M. Leckie (2009), Early history of the Western Pacific Warm Pool during the middle to late Miocene (~13.2–5.8 Ma): Role of sea-level change and implications for equatorial circulation, *Palaeogeogr. Palaeoclimatol. Palaeoecol.*, *274*, 140–159.

Nehrke, G., N. Keul, G. Langer, L. J. de Nooijer, J. Bijma, and A. Meibom (2013), A new model for biomineralization and trace-element signatures of Foraminifera tests, *Biogeosciences*, *10*, 6759–6767, doi:10.5194/bg-10-6759-2013.

Passchier, S., G. Browne, B. Field, C. R. Fielding, L. A. Krissek, K. Panter, S. F. Pekar, and ANDRILL-SMS Science Team (2011), Early and middle Miocene Antarctic glacial history from the sedimentary facies distribution in the AND-2A drill hole, Ross Sea, Antarctica, *Geol. Soc. Am. Bull.*, doi:10.1130/B30334.1.

Pedersen, T. F., and N. B. Price (1982), The geochemistry of manganese carbonate in Panama Basin sediments, *Geochim. Cosmochim. Acta*, *46*, 59–68.

Raitzsch, M., A. Duenas-Bohorquez, G.-J. Reichart, L. J. de Nooijer, and T. Bickert (2010), Incorporation of Mg and Sr into calcite of cultured benthic foraminifera: Impact of calcium concentration and associated calcite saturation state, *Biogeosciences*, *7*, 869–881.

Rathmann, S., and H. Kuhnert (2008), Carbonate ion effect on Mg/Ca, Sr/Ca and stable isotopes on the benthic foraminifera *Oridorsalis umbonatus* off Namibia, *Mar. Micropaleontol.*, *66*, 120–133, doi:10.1016/j.marmicro.2007.08.001.

Rathmann, S., S. Hess, H. Kuhnert, and S. Mulitza (2004), Mg/Ca ratios of the benthic foraminifera *Oridorsalis umbonatus* obtained by laser ablation from core top sediments: Relationship to bottom water temperature, *Geochem. Geophys. Geosyst.*, *5*, Q12013, doi:10.1029/2004GC000808.

Ravelo, A. C., and D. H. Andreasen (2000), Enhanced circulation during a warm period, *Geophys. Res. Lett.*, *27*, 1001–1004, doi:10.1029/1999GL007000.

Raymo, M. E., W. F. Ruddiman, J. Backman, B. M. Clement, and D. G. Martinson (1989), Late Pliocene variation in Northern Hemisphere ice sheets and North Atlantic deep water circulation, *Paleoceanography*, *4*, 413–446, doi:10.1029/PA004i004p00413.

Ries, J. B. (2004), Effect of ambient Mg/Ca ratio on Mg fractionation in calcareous marine invertebrates: A record of the oceanic Mg/Ca ratio over the Phanerozoic, *Geology*, *32*, 981–984, doi:10.1130/G20851.1.

Rohling, E. J., G. L. Foster, K. M. Grant, G. Marino, A. P. Roberts, M. E. Tamisiea, and F. Williams (2014), Sea-level and deep-sea-temperature variability over the past 5.3 million years, *Nature*, *508*, 477–482.

Rosenthal, Y., E. A. Boyle, and N. Slowey (1997), Temperature control on the incorporation of magnesium, strontium, fluorine, and cadmium into benthic foraminiferal shells from Little Bahama Bank: Prospects for thermocline paleoceanography, *Geochim. Cosmochim. Acta*, *61*, 3633–3643, doi:10.1016/S0016-7037(97)00181-6.

Rosenthal, Y., C. H. Lear, D. W. Oppo, and B. K. Linsley (2006), Temperature and carbonate ion effects on Mg/Ca and Sr/Ca ratios in benthic foraminifera: Aragonitic species *Hoeglundina elegans*, *Paleoceanography*, *21*, PA1007, doi:10.1029/2005PA001158.

Scher, H. D., S. M. Bohaty, J. C. Zachos, and M. L. Delaney (2011), Two-stepping into the icehouse: East Antarctic weathering during progressive ice-sheet expansion at the Eocene-Oligocene transition, *Geology*, *39*, 383–386.

Schmidt, M. W., M. J. Vautravers, and H. J. Spero (2006), Western Caribbean sea surface temperatures during the late Quaternary, *Geochem. Geophys. Geosyst.*, *7*, Q02P10, doi:10.1029/2005GC000957.

Segev, E., and J. Erez (2006), Effect of Mg/Ca ratio in seawater on shell composition in shallow benthic foraminifera, *Geochem. Geophys. Geosyst.*, *7*, Q02P09, doi:10.1029/2005GC000969.

Shackleton, N. J., and J. P. Kennett (1975), Paleotemperature history of the Cenozoic and the initiation of Antarctic glaciation: Oxygen and carbon isotope analyses in DSDP Sites 277, 279, and 281, *Initial Rep. Deep Sea Drill. Proj.*, *29*, 743–755.

Shevenell, A. E., J. P. Kennett, and D. W. Lea (2008), Middle Miocene ice sheet dynamics, deep-sea temperatures, and carbon cycling: A Southern Ocean perspective, *Geochem. Geophys. Geosyst.*, *9*, Q02006, doi:10.1029/2007GC001736.

Thiede, J., A. Winkler, T. Wolf-Welling, O. Eldholm, A. M. Myhre, K.-H. Baumann, R. Henrich, and R. Stein (1998), Late Cenozoic history of the polar North Atlantic: Results from ocean drilling, *Quat. Sci. Rev.*, *17*, 185–208.

Thomas, E. (1998), The biogeography of the late Paleocene benthic foraminiferal extinction, in *Late Paleocene-Early Eocene Biotic and Climatic Events in the Marine and Terrestrial Records*, edited by M.-P. Aubry, S. Lucas, and W. A. Berggren, pp. 214–243, Columbia Univ. Press, New York.

Thomas, E., and N. J. Shackleton (1996), The Palaeocene-Eocene benthic foraminiferal extinction and stable isotope anomalies, *Geol. Soc. London Spec. Publ.*, *101*, 401–441.

Tisserand, A. A., T. M. Dokken, C. Waelbroeck, J.-M. Gherardi, V. Scao, C. Fontanier, and F. Jorissen (2013), Refining benthic foraminiferal Mg/Ca-temperature calibrations using core-tops from the western tropical Atlantic: Implication for paleotemperature estimation, *Geochem. Geophys. Geosyst.*, *14*, 929–946, doi:10.1002/ggge.20043.

Wade, B. S., P. N. Pearson, W. A. Berggren, and H. Pälike (2011), Review and revision of Cenozoic tropical planktonic foraminiferal biostratigraphy and calibration to the geomagnetic polarity and astronomical time scale, *Earth Sci. Rev.*, *104*(1–3), 111–142, doi:10.1016/j.earscirev.2010.09.003.

Wilson, D. S., D. Pollard, R. M. DeConto, S. S. R. Jamieson, and B. P. Luyendyk (2013), Initiation of the West Antarctic ice sheet and estimates of total Antarctic ice volume in the earliest Oligocene, *Geophys. Res. Lett.*, *40*, 4305–4309, doi:10.1002/grl.50797.

Yu, J., and H. Elderfield (2007), Benthic foraminiferal B/Ca ratios reflect deep water carbonate saturation state, *Earth Planet. Sci. Lett.*, *258*, 73–86.
Yu, J., and H. Elderfield (2008), Mg/Ca in the benthic foraminifera *Cibicidoides wuellerstorfi* and *Cibicidoides mundulus*: Temperature versus carbonate ion saturation, *Earth Planet. Sci. Lett.*, *276*, 129–139.
Yu, J., H. Elderfield, M. Greaves, and J. Day (2007), Preferential dissolution of benthic foraminiferal calcite during laboratory reductive cleaning, *Geochem. Geophys. Geosyst.*, *8*, Q06016, doi:10.1029/2006GC001571.
Zachos, J., M. Pagani, L. Sloan, E. Thomas, and K. Billups (2001), Trends, rhythms, and aberrations in global climate 65 Ma to present, *Science*, *292*, 686–693.
Zachos, J. C., J. R. Breza, and S. W. Wise (1992), Early Oligocene ice-sheet expansion on Antarctica: Stable isotope and sedimentological evidence from Kerguelen Plateau, southern Indian Ocean, *Geology*, *20*, 569–573.
Zachos, J. C., T. M. Quinn, and K. Salamy (1996), High resolution (10^4 years) deep-sea foraminiferal stable isotope time series, *Paleoceanography*, *11*, 251–266, doi:10.1029/96PA00571.
Zachos, J. C., G. R. Dickens, and R. E. Zeebe (2008), An early Cenozoic perspective on greenhouse warming and carbon-cycle dynamics, *Nature*, *451*, 279–283, doi:10.1038/nature06588.
Zeebe, R. E. (2007), Modeling CO_2 chemistry, $\delta^{13}C$, and oxidation of organic carbon and methane in sediment prewater: Implications for paleo-proxies in benthic foraminifera, *Geochim. Cosmochim. Acta*, *71*, 3238–3256.
Zeebe, R. E., and J. C. Zachos (2007), Reversed deep-sea carbonate ion basin gradient during Paleocene-Eocene thermal maximum, *Paleoceanography*, *22*, PA3201, doi:10.1029/2006PA001395.
Zhang, Y. G., M. Pagani, and Z. Liu (2014), A 12-million-year temperature history of the tropical Pacific Ocean, *Science*, *344*, 84–87.
Zhang, Z., K. H. Nisancioglu, F. Flatøy, M. Bentsen, I. Bethke, and H. Wang (2011), Tropical seaways played a more important role than high latitude seaways in Cenozoic cooling, *Clim. Past*, *7*, 801–813.